


# Scalable mixed-domain Gaussian process modeling and model reduction for longitudinal data

Juho Timonen\*  and Harri Lähdesmäki\*

**Abstract.** Gaussian process (GP) models that combine both categorical and continuous input variables have found use in analysis of longitudinal data and computer experiments. However, standard inference for these models has the typical cubic scaling, and common scalable approximation schemes for GPs cannot be applied since the covariance function is non-continuous. In this work, we derive a basis function approximation scheme for mixed-domain covariance functions, which scales linearly with respect to the number of observations and total number of basis functions. The proposed approach is naturally applicable to also Bayesian GP regression with discrete observation models. We demonstrate the scalability of the approach and compare model reduction techniques for additive GP models in a longitudinal data context. We confirm that we can approximate the exact GP model accurately in a fraction of the runtime compared to fitting the corresponding exact model. In addition, we demonstrate a scalable model reduction workflow for obtaining smaller and more interpretable models when dealing with a large number of candidate predictors.

**MSC2020 subject classifications:** Primary 60G15, 62-08.

**Keywords:** Gaussian processes, Longitudinal data, Scalable methods, Model reduction.

## 1 Introduction

Gaussian processes (GPs) offer a flexible nonparametric way of modeling unknown functions. While Gaussian process regression and classification are commonly used in problems where the domain of the unknown function is continuous, recent work has seen use of GP models also in mixed domains, where some of the input variables are categorical or discrete and some are continuous. Applications of mixed-domain GPs are found e.g. in Bayesian optimization (Garrido-Merchán and Hernández-Lobato, 2020), computer experiments (Qian et al., 2008; Deng et al., 2017; Roustant et al., 2020; Wang et al., 2021; Zhang and Notz, 2015) and longitudinal data analysis (Cheng et al., 2019; Timonen et al., 2021). For example in biomedical applications, the modeled function often depends on categorical covariates, such as treatment vs. no treatment, and accounting for such time-varying effects is essential. Non-trivial mixed-domain kernels are required in order to obtain an interpretable model with both shared and category-specific effects (Timonen et al., 2021).

Since all commonly used kernel functions (i.e. covariance functions) are defined for either purely continuous or purely categorical input variables, kernels for mixed-domain

---

\*Department of Computer Science, Aalto University, [juho.timonen@aalto.fi](mailto:juho.timonen@aalto.fi); [harri.lahdesmaki@aalto.fi](mailto:harri.lahdesmaki@aalto.fi)

GPs are typically obtained by combining continuous and categorical kernels through multiplication. Additional modeling flexibility can be obtained by summing the product kernels as has been done in the context of GP modeling for longitudinal data (Cheng et al., 2019; Timonen et al., 2021).

It is well known that exact GP regression has a theoretical complexity of  $\mathcal{O}(N^3)$  and requires  $\mathcal{O}(N^2)$  memory, where  $N$  is the number of observations. This poses a computational problem which in practice renders applications of exact GP regression infeasible for large data. Various scalable approximation approaches for GPs have been proposed (see e.g. (Liu et al., 2020) for a review). However, many popular approaches, such as the inducing point (Snelson and Ghahramani, 2006; Titsias, 2009) and kernel interpolation (Wilson and Nickisch, 2015) methods, can only be applied directly if the kernel (i.e. covariance) function is continuous and differentiable. In addition, they typically require the Gaussian observation model, which is not appropriate for modeling for example discrete, categorical or ordinal response variables. See Sec. 3 for a review of previous methods.

In the presence of a variety of possible explanatory covariates, reducing the model to a minimal set of variables can be an essential part of building an interpretable and a useful model. The combinatorial explosion of possible alternative models as a function of the number of candidate covariates poses an additional problem for scalable modeling workflow that aims to produce a small an interpretable model with good predictive properties.

In this work, we present a scalable approximation and model reduction scheme for additive mixed-domain GPs, where the covariance structure depends on both continuous and categorical variables. We extend the Hilbert space reduced-rank approximation (Solin and Särkkä, 2020) for said additive mixed-domain GPs, making it applicable to e.g. analysis of large longitudinal data sets. The approach scales linearly with respect to data set size and allows a wide variety of categorical kernels that specify possible correlation over groups. It allows an arbitrary observation model and full Bayesian inference for the model hyperparameters, and is suitable for longitudinal data as it allows product kernels of continuous and categorical kernels for modeling for example group-specific effects that sum to zero. Furthermore, we demonstrate how to use the projection predictive technique (see e.g. (Pavone et al., 2020)) for said models and compare it with a variance decomposition based covariate relevance assessment technique (Timonen et al., 2021) to obtain recommendations how to efficiently produce small and interpretable additive GP models for longitudinal data. We offer an open source R package (R Core Team, 2023) called `lgpr2`<sup>1</sup> that implements the described longitudinal approximate GP models and model reduction techniques.

---

<sup>1</sup><https://github.com/jtimonen/lgpr2>

## 2 Background

### 2.1 Gaussian processes

A Gaussian process (GP) is a collection of random variables, any finite number of which has a multivariate normal distribution (Rasmussen and Williams, 2006). A function  $f$  is a GP

$$f \sim \mathcal{GP}(m(\mathbf{x}), k(\mathbf{x}, \mathbf{x}')) \quad (1)$$

with mean function  $m(\mathbf{x})$  and kernel (or covariance) function  $k(\mathbf{x}, \mathbf{x}')$ , if for any finite number of inputs  $\{\mathbf{x}_i \in \mathcal{X}\}_{i=1}^N$ , the vector of function values  $\mathbf{f} = [f(\mathbf{x}_1), \dots, f(\mathbf{x}_N)]^\top$  follows a multivariate normal distribution  $\mathbf{f} \sim \mathcal{N}(\mathbf{m}, \mathbf{K})$  with mean vector  $\mathbf{m} = [m(\mathbf{x}_1), \dots, m(\mathbf{x}_N)]^\top$  and  $N \times N$  covariance matrix  $\mathbf{K}$  with entries  $\{\mathbf{K}\}_{nm} = k(\mathbf{x}_n, \mathbf{x}_m)$ . The mean function is commonly the constant zero function  $m(\mathbf{x}) = 0$ , and we have this convention throughout the paper. The kernel function encodes information about the covariance of function values at different points, and therefore affects the model properties crucially.

### 2.2 Bayesian GP regression

In GP regression, the conditional distribution of response variable  $y$  given covariates  $\mathbf{x}$  is modeled as some parametric distribution  $p(y \mid f(\mathbf{x}), \boldsymbol{\theta}_{\text{obs}})$ , where  $\boldsymbol{\theta}_{\text{obs}}$  represents possible parameters of the observation model. The function  $f$  has a zero-mean GP prior with covariance function  $k(\mathbf{x}, \mathbf{x}' \mid \boldsymbol{\theta}_{\text{GP}})$  that has hyperparameters  $\boldsymbol{\theta}_{\text{GP}}$ . We focus on Bayesian GP modeling, where in addition to the GP prior for  $f$ , we have a parameter prior distribution  $p(\boldsymbol{\theta})$  for  $\boldsymbol{\theta} = \{\boldsymbol{\theta}_{\text{GP}}, \boldsymbol{\theta}_{\text{obs}}\}$ . Given  $N$  observations  $\mathcal{D} = \{y_n, \mathbf{x}_n\}_{n=1}^N$  our goal is to infer the posterior

$$p(\boldsymbol{\theta}, \mathbf{f} \mid \mathcal{D}) \propto p(\boldsymbol{\theta}, \mathbf{f}) \cdot p(\mathbf{y} \mid \mathbf{f}, \boldsymbol{\theta}), \quad (2)$$

where  $\mathbf{y} = [y_1, \dots, y_N]^\top$ . The part

$$p(\boldsymbol{\theta}, \mathbf{f}) = p(\mathbf{f} \mid \boldsymbol{\theta}) \cdot p(\boldsymbol{\theta}) \quad (3)$$

is the prior and

$$p(\mathbf{y} \mid \mathbf{f}, \boldsymbol{\theta}) = \prod_{n=1}^N p(y_n \mid f(\mathbf{x}_n), \boldsymbol{\theta}_{\text{obs}}) \quad (4)$$

is the likelihood. This task often has to be done by sampling from  $p(\boldsymbol{\theta}, \mathbf{f} \mid \mathcal{D})$  using MCMC methods, which requires evaluating the right-hand side of Eq. 2 (and possibly its gradient) thousands of times. As the likelihood and parameter prior usually are independent over each parameter and data point, they scale linearly and are not a bottleneck. Instead, computing the GP prior density

$$p(\mathbf{f} \mid \boldsymbol{\theta}) = \mathcal{N}(\mathbf{f} \mid \mathbf{0}, \mathbf{K}), \quad (5)$$

where the  $N \times N$  matrix  $\mathbf{K}$  has entries  $\{\mathbf{K}\}_{nm} = k(\mathbf{x}_n, \mathbf{x}_m \mid \boldsymbol{\theta}_{\text{GP}})$ , is a costly operation as evaluating the (log) density of the  $N$ -dimensional multivariate normal distribution has

generally  $\mathcal{O}(N^3)$  complexity (see Sec. S3.6). Furthermore, the matrix  $\mathbf{K}$  takes  $\mathcal{O}(N^2)$  memory.

An often exploited fact is that if the observation model (and therefore likelihood) is Gaussian,  $\mathbf{f}$  can be analytically marginalized and only the marginal posterior  $p(\boldsymbol{\theta} \mid \mathcal{D})$  needs to be sampled. This reduces the MCMC dimension by  $N$  and likely improves sampling efficiency, but one however needs to evaluate  $p(\mathbf{y} \mid \boldsymbol{\theta})$  which is again an  $N$ -dimensional multivariate Gaussian. The  $\mathcal{O}(N^3)$  complexity and  $\mathcal{O}(N^2)$  memory requirements therefore remain. In this paper, we generally assume an arbitrary observation model, and defer the details of the Gaussian observation model until Sec. S3.2.

### 2.3 Additive GP regression

In additive GP regression, the modeled function  $f$  consists of additive components so that  $f = f^{(1)} + \dots + f^{(J)}$ , and each component  $j = 1, \dots, J$  has a GP prior

$$f^{(j)} \sim \mathcal{GP}(0, k_j(\mathbf{x}, \mathbf{x}')), \quad (6)$$

independently from other components. This means that the total GP prior is  $f \sim \mathcal{GP}(0, k(\mathbf{x}, \mathbf{x}'))$  with

$$k(\mathbf{x}, \mathbf{x}') = \sum_{j=1}^J k_j(\mathbf{x}, \mathbf{x}'). \quad (7)$$

Furthermore,  $\mathbf{f}^{(j)} \sim \mathcal{N}(\mathbf{0}, \mathbf{K}^{(j)})$  for each vector

$$\mathbf{f}^{(j)} = \left[ f^{(j)}(\mathbf{x}_1), \dots, f^{(j)}(\mathbf{x}_N) \right]^\top, \quad (8)$$

where  $j = 1, \dots, J$ . The matrix  $\mathbf{K}^{(j)}$  is defined so that its elements are  $\{\mathbf{K}^{(j)}\}_{nm} = k_j(\mathbf{x}_n, \mathbf{x}_m)$ . This means that the prior for  $\mathbf{f} = \mathbf{f}^{(1)} + \dots + \mathbf{f}^{(J)}$  is  $\mathbf{f} \sim \mathcal{N}(\mathbf{0}, \mathbf{K})$ , where  $\mathbf{K} = \sum_{j=1}^J \mathbf{K}^{(j)}$ .

In additive GP models, we are often ultimately interested in inferring the components  $\mathbf{f}^{(j)}$ , in which case Bayesian inference requires sampling all  $\mathbf{f}^{(j)}$ . Adding one component increases the number of parameters by  $N$  (plus the possible additional kernel hyperparameters). Moreover, the multivariate normal prior (Eq. 5) needs to be evaluated for each component, adding the computational burden. In the case of Gaussian likelihood, adding more components does not add any multivariate normal density evaluations as it still needs to be done only for  $p(\mathbf{y} \mid \boldsymbol{\theta})$ . Also the marginal posteriors of each  $\mathbf{f}^{(j)}$  are analytically available (see Sec. S3.2).

### 2.4 Mixed-domain kernels for longitudinal data

Longitudinal data is common in biomedical, psychological, social and other studies and consists of multiple measurements of several subjects at multiple time points. In addition to time (often expressed as subject age), other continuous covariates can be measured. Moreover, in addition to subject id, other categorical covariates, such as

treatment, sex or country can be available. In the statistical methods literature, such data is commonly modeled using generalized linear mixed effect models (Verbeke and Molenberghs, 2000). In recent work (Cheng et al., 2019; Quintana et al., 2016; Timonen et al., 2021), longitudinal data has been modeled using additive GPs, where, similar to commonly used linear models, each component  $f^{(j)}$  is a function of at most one categorical and one continuous variable. Each variable is assigned a one-dimensional base kernel and for components that contain both a continuous and categorical kernel, the kernel  $k_j$  is their product. As the total kernel  $k$  is composed of the simpler categorical and continuous kernels through multiplication and addition, it has a mixed domain.

These models have the very beneficial property that the effects of individual covariates are interpretable. The marginal posterior distributions of each component can be studied to infer the marginal effect of different covariates. As an example, if  $k_j$  is just the exponentiated quadratic (EQ) kernel

$$k_{\text{EQ}}(x, x') = \alpha^2 \exp\left(-\frac{(x - x')^2}{2\ell^2}\right) \quad (9)$$

and  $x$  is age, the component  $f_j$  can be interpreted as the shared effect of age. On the other hand, if  $k_j$  is the product kernel  $k_{\text{EQ} \times \text{ZS}}((x, z), (x', z')) = k_{\text{EQ}}(x, x')k_{\text{ZS}}(z, z')$  where

$$k_{\text{ZS}}(z, z') = \begin{cases} 1 & \text{if } z = z' \\ -\frac{1}{C-1} & \text{if } z \neq z' \end{cases} \quad (10)$$

is the zero-sum (ZS) kernel (Kaufman and Sain, 2010) for a categorical variable  $z$  that has  $C > 1$  categories,  $f^{(j)}$  can be interpreted as the category-specific effect of the continuous covariate  $x$ . This also has the property that the effect sums to zero over categories at all values for  $x$  (see Timonen et al. (2021) for proof), which helps in separating the category effect from the shared effect, if a model has both.

### 3 Related research

**GPs and categorical inputs** A suggested approach to handle GPs with categorical covariates is to use a one-hot encoding which turns a variable with  $C$  categories into  $C$  binary variables, of which only one is on at a time, and then apply a continuous kernel for them. Garrido-Merchán and Hernández-Lobato (2020) highlight that the resulting covariance structure is problematic because it does not take into account that only one of the binary variables can be one at a time. This poorly motivated approach might have originated merely from the fact that common GP software have lacked support for categorical kernels. We find it more sensible to define kernels directly on categorical covariates, as that way we can always impose the desired covariance structure.

Category-specific effects of a continuous covariate  $x$  can be achieved also by assigning independent GPs for the different categories. This way we have only continuous kernel functions, and can possibly use scalable approaches that are designed for them. This limited approach however cannot define any additional covariance structure between the categories, such as the zero-sum constraint (Eq. 10). The ZS kernel is a special case

of compound symmetry (CS), and for example Roustant et al. (2020) concluded that a CS covariance structure was more justified than using only independent GPs in their nuclear engineering application.

Chung et al. (2020) developed a deep mixed-effect GP model that facilitates individual-specific effects and scales as  $\mathcal{O}(PT^3)$ , where  $P$  is the number of individuals and  $T$  is the number of time points. Zhang et al. (2020) handled categorical inputs by mapping them to a continuous latent space and then using a continuous kernel. While this approach can detect interesting covariance structures, it does not remove need to perform statistical modeling with a predefined covariance structure as in Sec. 2.4. Another related non-parametric way to model group effects is to use hierarchical generalized additive models (Pedersen et al., 2019), as smoothing splines can be seen as a special case of GP regression (Kimeldorf and Wahba, 1970).

**Computer experiments** In analysis of computer experiments (Sacks et al., 1989), GPs can be used as a surrogate model for the output of a computer code that takes a long time to run. Often, both qualitative and quantitative factors affect the output of a computer code. Whereas the kernels used in this paper are valid by construct, a strategy to find general valid covariance functions for computer experiments involving both continuous and categorical variables was developed by Qian et al. (2008), using semidefinite programming. The output of the computer code can be assumed to be observed exactly, meaning that there is no model for the observation noise (Sec. 2.2). In this case, the presented approximation methodology can still be used via the strategy detailed in Sec. S3.3. with  $\sigma^2 = 0$ , as no noise can be seen as a special case of the Gaussian observation model with  $\sigma^2 \rightarrow 0$ .

**Scalable GP approximations** A number of approximation methods exist that reduce the complexity of GP regression to  $\mathcal{O}(N \cdot M^2)$ , where  $M$  controls the accuracy of the approximation. Popular approaches rely on global sparse approximations (Quiñonero Candela and Rasmussen, 2005) of the  $N \times N$  covariance matrix between all pairs of data points, using  $M$  inducing points. The locations of these inducing points are generally optimized using gradient-based continuous optimization simultaneously with model hyperparameters, which cannot be applied when the domain is not continuous. In Fortuin et al. (2021), the inducing-point approach was studied in purely discrete domains and Cao et al. (2015) presented an optimization algorithm that alternates between discrete optimization of inducing points, and continuous optimization of the hyperparameters. Disadvantages of this method are that it cannot find inducing points outside of the training data, does not perform full Bayesian inference for the hyperparameters, and assumes a Gaussian observation model.

A Hilbert space basis function approach for reduced-rank GP approximation in continuous domains, on which this work is based, was proposed by Solin and Särkkä (2020). Its use in the practice in the Bayesian setting was studied more in Riutort-Mayol et al. (2022).

## 4 Mixed-domain covariance function approximation

### 4.1 Basic idea

We continue with the notation established in Sec. 2, and note that  $\mathbf{x}$  denotes a general input that can consist of both continuous and categorical dimensions. We consider approximations  $\mathbf{f} \approx \tilde{\mathbf{f}}$  that decompose the GP kernel function as

$$k(\mathbf{x}, \mathbf{x}') \approx \tilde{k}(\mathbf{x}, \mathbf{x}') = \sum_{m=1}^M \psi_m(\mathbf{x})\psi_m(\mathbf{x}'), \quad (11)$$

where functions  $\psi_m$  have to be designed so that the approximation is accurate but easy to compute. This is useful in GP regression, because we get a low-rank approximate decomposition for the kernel matrix  $\mathbf{K} \approx \tilde{\mathbf{K}} = \mathbf{\Psi}\mathbf{\Psi}^\top$ , where  $\mathbf{\Psi}$  is the  $N \times M$  matrix with elements  $[\mathbf{\Psi}]_{n,m} = \psi_m(\mathbf{x}_n)$ . Using this approximation, we can write the approximate GP prior  $\tilde{\mathbf{f}} \sim \mathcal{N}(\mathbf{0}, \mathbf{\Psi}\mathbf{\Psi}^\top)$  using  $M$  parameters  $\xi_m$  with independent standard normal priors, connected to  $\mathbf{f}$  through the reparametrization  $\tilde{\mathbf{f}} = \mathbf{\Psi}\boldsymbol{\xi}$ , where  $\boldsymbol{\xi} = [\xi_1, \dots, \xi_M]^\top$ . Evaluating the prior density  $p(\boldsymbol{\xi}) = \prod_{m=1}^M \mathcal{N}(\xi_m | 0, 1)$  has now only  $\mathcal{O}(M)$  cost. After obtaining posterior draws of  $\boldsymbol{\xi}$ , we can obtain posterior draws of  $\tilde{\mathbf{f}}$  with  $\mathcal{O}(NM)$  cost, which comes from computing the matrix  $\mathbf{\Psi}$ . The likelihood (Eq. 4) can then be evaluated one data point at a time and the total complexity of the approach is only  $\mathcal{O}(NM + M)$ . Furthermore, the memory requirement is reduced from  $\mathcal{O}(N^2)$  to  $\mathcal{O}(NM)$ , since we only need to store  $\mathbf{\Psi}$  and never compute  $\mathbf{K}$ . This is the approach used throughout this paper, and the focus is on how to design the functions  $\psi_m$  for different kernel functions so that the approximation is accurate with  $M \ll N$ .

### 4.2 Continuous isotropic covariance functions

A continuous stationary covariance function  $k(\mathbf{x}, \mathbf{x}') : \mathbb{R}^D \times \mathbb{R}^D \rightarrow \mathbb{R}$  depends only on the difference  $\mathbf{r} = \mathbf{x} - \mathbf{x}'$  and can therefore be written as  $k(\mathbf{r})$ . Such covariance functions can be approximated by methods that utilize the spectral density

$$S(\omega) = \int k(\mathbf{r}) e^{-i\omega^\top \mathbf{r}} d\mathbf{r}. \quad (12)$$

If the covariance function is isotropic, meaning that it depends only on the Euclidean norm  $\|\mathbf{r}\|$ , also  $S(\omega)$  is isotropic and can be written as  $S(\|\omega\|)$ , i.e. as a function of one variable. As shown in (Solin and Särkkä, 2020), an isotropic covariance function can be approximated as

$$\tilde{k}(\mathbf{x}, \mathbf{x}') = \sum_{b=1}^B s_b \phi_b(\mathbf{x}) \phi_b(\mathbf{x}'), \quad (13)$$

where  $s_b = S(\sqrt{\lambda_b})$  and  $\phi_b$  and  $\lambda_b$  are the  $B$  first eigenfunctions and eigenvalues of the Dirichlet boundary value problem

$$\begin{cases} \frac{\partial^2}{\partial \mathbf{x}^2} \phi_b(\mathbf{x}) &= \lambda_b \phi_b(\mathbf{x}), & \mathbf{x} \in \Omega \\ \phi_b(\mathbf{x}) &= 0, & \mathbf{x} \in \partial\Omega \end{cases} \quad (14)$$

for a compact set  $\Omega \subset \mathbb{R}^D$ . We see that this approximation has the same form as Eq. 11 with  $M = B$  and  $\psi_m(\mathbf{x}) = \sqrt{s_m}\phi_m(\mathbf{x})$ . The spectral density has a closed form for many kernels, and the domain  $\Omega$  can be selected so that the eigenvalues and eigenfunctions have one too. Functions  $\psi_m(\mathbf{x})$  are therefore easy to evaluate and the computation strategy described in Sec. 4.1 can then be used. As an example, when  $D = 1$  and  $\Omega = [-L, L]$  with  $L > 0$ , we have

$$\begin{cases} \phi_b(\mathbf{x}) &= \frac{1}{\sqrt{L}} \sin\left(\frac{\pi b(\mathbf{x}+L)}{2L}\right) \\ \lambda_b &= \left(\frac{\pi b}{2L}\right)^2 \end{cases}. \quad (15)$$

and it was proven in (Solin and Särkkä, 2020) that in this case  $\lim_{L \rightarrow \infty} [\lim_{B \rightarrow \infty} \tilde{k}(\mathbf{x}, \mathbf{x}')] = k(\mathbf{x}, \mathbf{x}')$  uniformly for any stationary  $k$  that has a regular enough spectral density. For example for the EQ kernel (Eq. 9)  $k_{\text{EQ}}(r) = \alpha^2 \exp\left(-\frac{r^2}{2\ell^2}\right)$ , the spectral density is  $S_{\text{EQ}}(\omega) = \alpha^2 \ell \sqrt{2\pi} \exp\left(-\frac{\ell^2 \omega^2}{2}\right)$ .

### 4.3 Kernels for categorical variables

#### Eigendecomposition

Let us study a kernel  $k : \mathcal{X} \times \mathcal{X} \rightarrow \mathbb{V} \subset \mathbb{R}$ , where  $\mathcal{X}$  is a finite set of  $C$  possible values (categories). We can encode these categories numerically as integers  $\mathcal{X} = \{1, \dots, C\}$ . Because there are only  $C^2$  possible input combinations  $(v, w)$  for  $k$ , and therefore  $|\mathbb{V}| \leq C^2$ , we can list them in the  $C \times C$  matrix  $\mathbf{C}$  which has elements  $[\mathbf{C}]_{v,w} = k(v, w)$ . The symmetric square matrix  $\mathbf{C}$  has the orthogonal eigendecomposition

$$\mathbf{C} = \mathbf{\Theta} \mathbf{D} \mathbf{\Theta}^\top, \quad (16)$$

where  $\mathbf{D}$  is the diagonal matrix containing the eigenvalues  $d_c$ ,  $c = 1, \dots, C$  on the diagonal and  $\mathbf{\Theta}$  has the  $C$  eigenvectors as its columns. For each column  $c$ , we can define function  $\varphi_c : \mathcal{X} \rightarrow \mathbb{R}$  so that  $\varphi_c(v) = [\mathbf{\Theta}]_{v,c}$ . We see that

$$k(v, w) = [\mathbf{C}]_{v,w} = [\mathbf{\Theta} \mathbf{D} \mathbf{\Theta}^\top]_{v,w} \quad (17)$$

$$= \sum_{c=1}^C d_c [\mathbf{\Theta}]_{v,c} [\mathbf{\Theta}]_{w,c} = \sum_{c=1}^C d_c \varphi_c(v) \varphi_c(w), \quad (18)$$

meaning that we have written  $k$  in the form of Eq. 11 with  $M = C$  and  $\psi_m(\mathbf{x}) = \sqrt{d_m} \varphi_m(\mathbf{x})$ . Note that this is an exact function decomposition for  $k$  and not an approximation. The complexity of computing the eigendecomposition is  $\mathcal{O}(C^3)$ , but in typical applications  $C \ll N$  and this is not a bottleneck. Actually, for example for the ZS kernel and other CS kernels, the eigenvalues have a closed form and the corresponding eigenbasis is known (see next subsection). Furthermore, if  $k$  does not depend on any hyperparameters, the eigendecomposition only needs to be done once before parameter inference. If it is of type  $k(\mathbf{x}, \mathbf{x}') = \alpha^2 k_0(\mathbf{x}, \mathbf{x}')$  where  $\alpha$  is the only parameter, the decomposition can obviously be done just for  $k_0$  which again has no parameters. Evaluating functions  $\varphi_m$  is easy as it corresponds to just looking up a value from the matrix  $\mathbf{\Theta}$ .



### Compound symmetry kernels

For a categorical variable  $z$ , the compound symmetry (CS) (Pinheiro and Bates, 2000) kernel function is

$$k_{\text{CS}}(z, z' \mid \alpha, \rho) = \begin{cases} \alpha^2 & \text{if } z = z' \\ \rho & \text{if } z \neq z' \end{cases}, \quad (19)$$

meaning that all within-group variances  $\alpha^2 \geq 0$  are equal and all between-group covariances  $\rho$  are too. For  $z$  with  $C$  different categories, we need the restriction  $-\frac{\alpha^2}{C-1} \leq \rho \leq \alpha^2$  to ensure that  $k_{\text{CS}}(z, z' \mid \alpha, \rho)$  is positive semidefinite. By fixing  $\rho = -\frac{\alpha^2}{C-1}$ , we recover  $\alpha^2 k_{\text{ZS}}(z, z')$  as a special case.

The  $C \times C$  matrix  $\mathbf{C}$  that has elements  $\{\mathbf{C}\}_{v,w} = k_{\text{CS}}(v, w \mid \alpha, \rho)$  has eigenvalues

$$\begin{cases} d_1 &= \alpha^2 + (C-1)\rho \\ d_c &= \alpha^2 - \rho \end{cases} \quad c = 2, \dots, C \quad (20)$$

and the eigenvector corresponding to  $d_1$  is the vector of ones  $\mathbf{1}$ , and the eigenspace of  $d_c$ ,  $c \in \{2, \dots, C\}$ , is the orthogonal complement  $\mathbf{1}^\perp$  (Roustant et al., 2020). The decomposition  $\mathbf{C} = \mathbf{\Theta} \mathbf{D} \mathbf{\Theta}^\top$  can therefore be created for example so that the first column of  $\mathbf{\Theta}$  is  $\mathbf{1}$  normalized to unit length and remaining columns are normalized columns of the  $C \times (C-1)$  Helmert contrast matrix (Chambers and Hastie, 1992). The diagonal matrix  $\mathbf{D}$  has the eigenvalues  $d_c$ ,  $c = 1, \dots, C$  on its diagonal. For the ZS kernel, the eigenvalue  $d_1$  is zero, meaning that we actually have a rank  $C-1$  decomposition.

## 4.4 Mixed-domain product kernels

We now consider approximating a product kernel  $k(\mathbf{x}, \mathbf{x}') = \prod_{i=1}^P k_i(\mathbf{x}, \mathbf{x}')$  with  $\tilde{k}(\mathbf{x}, \mathbf{x}') = \prod_{i=1}^P \tilde{k}_i(\mathbf{x}, \mathbf{x}')$ , where for each  $\tilde{k}_i$  we have an available decomposition

$$\tilde{k}_i(\mathbf{x}, \mathbf{x}') = \sum_{m=1}^{M_i} \psi_{i,m}(\mathbf{x}) \psi_{i,m}(\mathbf{x}'), \quad (21)$$

which might be an approximation or an exact decomposition of  $k_i$ . The total approximation is

$$\tilde{k}(\mathbf{x}, \mathbf{x}') = \prod_{i=1}^P \sum_{m=1}^{M_i} \psi_{i,m}(\mathbf{x}) \psi_{i,m}(\mathbf{x}') \quad (22)$$

$$= \sum_{m_1=1}^{M_1} \dots \sum_{m_P=1}^{M_P} \psi_{m_1, \dots, m_P}^*(\mathbf{x}) \psi_{m_1, \dots, m_P}^*(\mathbf{x}') \quad (23)$$

where  $\psi_{m_1, \dots, m_P}^*(\mathbf{x}) = \prod_{i=1}^P \psi_{i, m_i}(\mathbf{x})$ . We have now a representation of the product kernel in the form of Eq. 11 with  $M = \prod_{i=1}^P M_i$  sum terms. Note that since the individual kernels in the product kernel can be both categorical and continuous, Eq. 23 provides

a kernel representation for mixed-domain GPs with product kernels. Also note that  $M$  grows exponentially with  $P$ .

An example with  $P = 2$  is the  $k_{\text{EQ} \times \text{ZS}}((x, z), (x', z'))$  interaction kernel (see Eq. 9-10), for which  $M_1 = B$ ,  $M_2 = C$ , and

$$\psi_{c,b}^*((x, z)) = \sqrt{s_b d_c} \phi_b(x) \varphi_c(z). \quad (24)$$

## 4.5 Mixed kernels for longitudinal data

In our framework, we consider mixed kernels  $k : \mathcal{X} \times \mathcal{X} \rightarrow \mathbb{R}$ , where  $\mathcal{X}$  is a mixed space of both continuous and categorical dimensions, consisting of multiplication and addition so that

$$k(\mathbf{x}, \mathbf{x}') = \sum_{j=1}^J \left( \prod_{q=1}^{Q_j} k_{j,q}(\mathbf{x}, \mathbf{x}') \prod_{r=1}^{R_j} \kappa_{j,r}(\mathbf{x}, \mathbf{x}') \right), \quad (25)$$

where each  $k_{j,q} : \mathbb{R} \times \mathbb{R} \rightarrow \mathbb{R}$  is isotropic and depends only on one continuous dimension of  $\mathbf{x}$  and each  $\kappa_{j,r} : \{1, \dots, C_{j,r}\} \rightarrow \mathbb{R}$  depends only on one categorical dimension of  $\mathbf{x}$ , which has  $C_{j,r}$  different categories. For each  $k_{j,q}$ , we use the basis function approximation (Eq. 13) with  $B_{j,q}$  basis functions and domain  $\Omega = [-L_{j,q}, L_{j,q}]$ , and for each  $\kappa_{j,r}$  the exact decomposition (Eq. 18). Using Eq. 22, we can obtain an approximation for the mixed domain kernel for longitudinal data shown in Eq. 25 that has the desired form  $\tilde{k}(\mathbf{x}, \mathbf{x}') = \sum_{m=1}^M \psi_m(\mathbf{x}) \psi_m(\mathbf{x}')$  (Eq. 11) using

$$M = \sum_{j=1}^J \left( \prod_{q=1}^{Q_j} B_{j,q} \prod_{r=1}^{R_j} C_{j,r} \right) \quad (26)$$

terms. In each term, the function  $\psi(\mathbf{x})$  is a product of  $Q_j$  factors  $\sqrt{s} \phi(\mathbf{x})$  and  $R_j$  factors  $\sqrt{d} \varphi(\mathbf{x})$ .

As an example, consider a commonly used additive longitudinal modeling approach where each additive term models the interaction effect for one continuous covariate and one categorical covariate, i.e.,  $Q_j = R_j = 1$  for each  $j$ . Assuming we use  $B_{j,1} = B$  basis functions for all components, then the scalability is  $\mathcal{O}(NM + M)$  where  $M = B \sum_{j=1}^J C_{j,1}$ . Further, if each categorical variable has  $C$  many different values, then the scalability is  $\mathcal{O}(NM + M)$ , where  $M = BJC$ .

## 4.6 Motivation and advice for base kernels

The used base kernels  $k_{j,q}$ ,  $\kappa_{j,r}$  should be selected so that they reflect the assumed covariance structure over the dimension of  $\mathbf{x}$  in question. In this paper we use the exponentiated quadratic kernel since we have observed it to work well enough, and its spectral density has a known closed form expression. The practitioner who wishes to use a different kernel needs to derive or look up its spectral density (Eq. 12). See for example (Rasmussen and Williams, 2006) for the formula for the spectral density of the Matern class of covariance functions.

For categorical variables we have used the zero-sum kernel because it solves a non-identifiability problem of additive population-level and group-level effects, as the group level effects sum to zero when the ZS kernel is used. Furthermore, the eigendecomposition (Eq. 16) of any kernel of the compound symmetry class has a convenient closed form expression (Sec. 4.3) and the ZS kernel is a valid compound symmetry kernel by definition. For a different categorical kernel, one may need to restrict its possible parameters so that positive semidefiniteness is ensured, and compute the corresponding eigendecomposition.

## 5 Model reduction

In many applications, a variety of potential explanatory variables are available and it is not known which should be included in the model. If the only goal is prediction, it can be useful to include all variables in the model. However, to reduce future measurement costs and improve interpretability, we often want to reduce the model as much as we can without losing predictive performance significantly. This is called *minimal subset variable selection* (Pavone et al., 2020). Compactly representing the data generating process is the goal also in *descriptive modeling* (Shmueli, 2010).

Here we compare two methods that are specifically suited for reducing the approximate additive GP models of longitudinal data, but have not been extensively highlighted in the longitudinal modeling literature. The model reduction problem is to select a subset of the components  $j \in \{1, \dots, J\}$  in the sum  $f = \sum_{j=1}^J f^{(j)}$ .

### 5.1 Additive variance decomposition

This method involves first fitting a full model  $\mathcal{M}_{\text{full}}$  with all candidate components included. The amount of noise  $p_{\text{noise}} \in (0, 1)$  is estimated from it using a variance decomposition similar to the Bayesian  $R^2$  (Gelman et al., 2019), and the remaining variance is decomposed between all the model components to obtain component relevances  $\text{rel}_j \in (0, 1 - p_{\text{noise}})$ , i.e.,  $p_{\text{noise}} + \sum_{j=1}^J \text{rel}_j = 1$ . The relevances can be used to rank the components from most important to least important, and the total explained variance (cumulative relevance) given a subset  $\mathcal{J} \subseteq \{1, \dots, J\}$  of components is

$$\text{rel}_{\mathcal{J}} = p_{\text{noise}} + \sum_{j \in \mathcal{J}} \text{rel}_j \quad (27)$$

The final reduced model can be selected to be the smallest subset that has, for example,  $\text{rel}_{\mathcal{J}} \geq 0.95$ .

Timonen et al. (2021) demonstrated that the method works well for exact longitudinal GP models, outperforming a cross-validation based method (Cheng et al., 2019) in assessing the covariate relevances. However, the experiments were done on data sets with a relatively low number of potential explanatory variables, and the experiments with simulated data did not involve correlated predictors.

## 5.2 Projection predictive model selection

### Overview

The projection predictive method (Goutis and Robert, 1998) is a model reduction method based on first fitting the best possible reference model  $\mathcal{M}_{\text{ref}}$ , which in our case will be the same as  $\mathcal{M}_{\text{full}}$  but does not generally need to be. For a given submodel  $\mathcal{M}_{\perp}$  containing a subset of the components, the submodel is fit by projecting the predictive distribution of  $\mathcal{M}_{\text{ref}}$  onto  $\mathcal{M}_{\perp}$ . This is done by minimizing KL divergence between the predictive distributions. In practice, the fit consists of MCMC draws and they have to be projected one by one. For models in the exponential family, this is equivalent to maximizing the likelihood of  $\mathcal{M}_{\perp}$  when the data is replaced by the prediction given by  $\mathcal{M}_{\text{ref}}$  (Pavone et al., 2020). A good reference model therefore is able to filter noise in the data, and therefore stabilize the model reduction process. A good theoretical explanation of why the reference model is helpful is given by Piironen et al. (2020).

The projection predictive technique cannot directly give a relevance value for each model component, and has to be coupled with a search through the subspace of alternative submodels. This gives a path through the submodel space, and some rule is then needed for final model size determination so that the predictive distribution of  $\mathcal{M}_{\text{sub}}$  is close enough to that of  $\mathcal{M}_{\text{ref}}$  (Piironen et al., 2020). An intuitive rule for deciding the reduced model size  $k$  is to pick the smallest  $k$  so that an estimated predictive utility, such as the expected log predictive density (ELPD), of the submodel is close to that of the reference model. Mathematically, this can be formulated as  $|\Delta_{\text{ELPD}}^k| \leq 1$ , where the relative difference in ELPD using model size  $k$  is

$$\Delta_{\text{ELPD}}^k = \frac{\hat{u}^* - \hat{u}_k}{s_k^*}, \quad (28)$$

where  $\hat{u}_k$  is the ELPD estimate for the submodel,  $\hat{u}^*$  is the ELPD estimate for the reference model, and  $s_k^*$  is the standard error for the reference model ELPD estimate. For other rules, see McLatchie et al. (2024).

For various types of models (Catalina et al., 2022; McLatchie et al., 2024; Piironen and Vehtari, 2017), the projection predictive technique has been shown to be able to find relatively small subsets of predictors that still have a good predictive power. The technique is fairly mature for generalized linear models (Piironen and Vehtari, 2017), but for complex types of models such as generalized linear mixed models and generalized additive (mixed) models (GAMs), it requires nontrivial tuning (Catalina et al., 2022).

### Application for approximate GP models of longitudinal data

The approximate additive GP models used in our experiments can be seen as GAMs, since the modeled function can be written as

$$f(\mathbf{x}) = \sum_{j=1}^J f^{(j)}(x_j, z_j) = \sum_{j=1}^J \sum_{b=1}^{B_j} w_{j,b} \phi_{j,b}(x_j) \quad (29)$$

where  $x_j$  is continuous<sup>2</sup>,  $z_j$  is a categorical factor, and the parameter  $w_{j,b}$  can be specific to group  $z_j$ . We note that shared effect terms are actually of the form  $f^{(j)}(x_j)$  and some terms may be only a category-specific offset, having the form  $f^{(j)}(z_j)$ .

GAM parameters are typically fitted by penalizing the likelihood with a wiggleness penalty term to avoid overfitting and Catalina et al. (2022) used similar penalization when applying the projection predictive method for GAMs. For exponential family models, projecting a reference model prediction  $f^*$  to submodel  $\mathcal{M}_\perp$  corresponds to finding coefficients  $w_{j,b}$  of the submodel that maximize the likelihood  $\mathcal{L}(f^* \mid \boldsymbol{\theta})$ . However, as this optimization problem is not identifiable, we instead maximize a penalized log likelihood

$$\mathcal{L}_\gamma(f^* \mid \boldsymbol{\theta}) = \log \mathcal{L}(f^* \mid \boldsymbol{\theta}) + \sum_{j \in \mathcal{M}_\perp} \gamma_j \int_{\Omega} \left[ \frac{\partial^2}{\partial x_j^2} f^{(j)}(x_j) \right]^2 dx_j, \quad (30)$$

where we have assumed  $f^{(j)}(x_j, z_j) = f^{(j)}(x_j)$  for simplicity. For how the categorical effects affect the penalization, we refer to Wood (2017), since we use the `gam()` function of the `mgcv` R package to solve the penalized optimization problem that performs the projection. This is achieved by defining a custom `smooth` that corresponds to the Hilbert space GP basis functions, and implementing the corresponding penalty for it. Submodel terms of the form

- $f^{(j)}(x_j)$  correspond to `s(x_j)`
- $f^{(j)}(z_j)$  correspond to `z_j`
- $f^{(j)}(x_j, z_j)$  correspond to `s(x_j, by = z_j) + z_j`

in the R formulas that we use with `gam()`. We use the "GCV.Cp" option to select the smoothing parameters  $\gamma_j$ .

Note that since the reference model fit consists of MCMC draws and the projection is done draw-by-draw, the penalised log likelihood optimization problem needs to be solved for the reference model predictions  $f^*$  computed using each draw. We use a subset of draws from the posterior to speed up the projection and be able to scale to larger sets of alternative submodels.

### Penalization for Hilbert space basis functions

We derive here the second derivative-based wiggleness penalty for the Hilbert space basis functions of the EQ kernel. Assume that the additive submodel has a term  $f_j$  modeled as an approximate GP (Eq. 13) with basis functions  $\phi_{j,b}(x) = \frac{1}{\sqrt{L}} \sin\left(\frac{\pi b(x+L)}{2L}\right)$ ,  $b = 1, \dots, B$  and domain  $\Omega = [-L, L]$ . The integral in the penalization term  $j$  in Eq. 30

---

<sup>2</sup>Note that  $x_j$  in the formula can be the same variable for many  $j$ , if both its shared and category-specific effects are modeled.

becomes

$$\int_{\Omega} [f''(x)]^2 dx = \int_{\Omega} \left[ \sum_{b=1}^B \sqrt{s_b} \phi_b''(x) \right]^2 dx, \quad (31)$$

where we have dropped the subscript  $j$  and superscript  $(j)$  for readability. We have

$$\phi_b''(x) = -\frac{(\pi b)^2}{(2L)^2} \cdot \phi_b(x) \quad (32)$$

and can write

$$\int_{\Omega} [f''(x)]^2 dx = \mathbf{w}^{\top} \mathbf{S} \mathbf{w}, \quad (33)$$

where

$$[\mathbf{S}]_{l,m} = \int_{\Omega} \phi_l''(x) \phi_m''(x) dx = 0 \quad (34)$$

for  $l \neq m$  and

$$[\mathbf{S}]_{b,b} = \left( \frac{\pi b}{2L} \right)^4 \quad (35)$$

on the diagonal. See derivation in Sec. S3.4. This means that basis functions with a higher frequency in the sine wave (larger  $b$ ) are penalized more.

## 6 Results

We confirm the scalability and accuracy of the presented approach using experiments with simulated and real data. Code for reproducing the experiments is publicly available <sup>3</sup>. In the same way as the earlier `lgpr` package (Timonen et al., 2021), the new R package `lgpr2` has a user-friendly interface based on the formula syntax in R and fits the described longitudinal approximate GP models using Stan (Carpenter et al., 2017).

In all experiments, used the same number of basis functions  $B$  for each approximate continuous kernel, and for all approximate components the same domain scaling factor  $c$ , which is defined so that  $\Omega = [-L, L]$  with  $L$  being  $c$  times the half-range of the continuous covariate of the approximated kernel (Riutort-Mayol et al., 2022). Additional experiment details are documented in Sec. S1.1.

### 6.1 Experiment 1: Simulation study

In the first experiment we create simulated longitudinal data consisting of categorical variables  $id$  and  $z$ , and a continuous variable  $age$ . We create data with 9 individuals, where individuals with  $id \in \{1, 4, 7\}$  belong to group  $z = 1$ , individuals with  $id \in$

---

<sup>3</sup><https://github.com/jtimonen/scalable-mixed-domain-GPs>

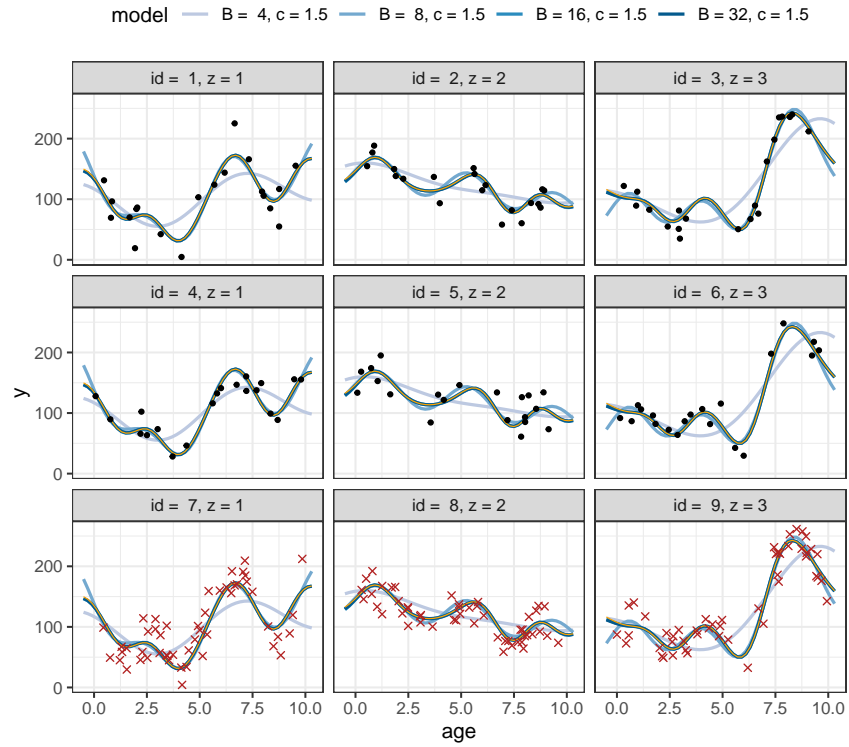


Figure 1: The posterior predictive mean for four different approximate models in one replication of Experiment 1. The models differ only based on the number of basis functions  $B$  and domain scaling factor  $c$ . The yellow line shows the posterior predictive mean for the corresponding exact GP model as a reference. Black dots are training data and red crosses test data.

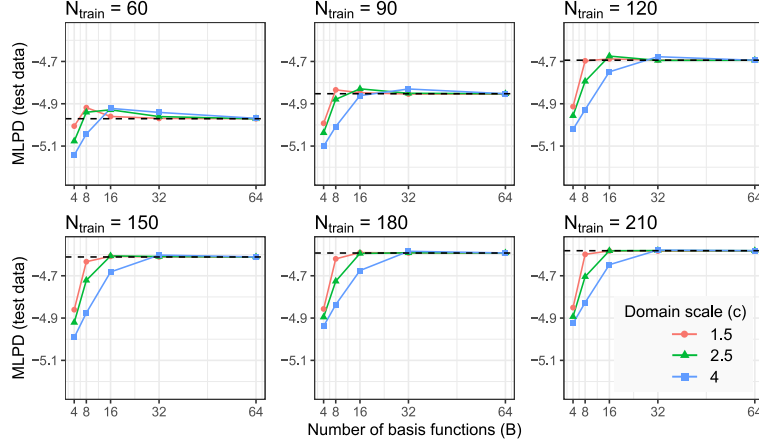


Figure 2: Mean log predictive density for test data in Experiment 1 for varying training data set sizes  $N_{\text{train}}$  and domain scales  $c$ . Black dashed line corresponds to the exact model. Results are averages over 30 replications of the experiment.

$\{2, 5, 8\}$  belong to group  $z = 2$  and individuals  $id \in \{3, 6, 9\}$  belong to group  $z = 3$ . For each individual 1-6, we create  $\frac{N_{\text{train}}}{6}$  observations at time points where  $age$  is drawn uniformly from the interval  $[0, 10]$ , and  $N_{\text{train}}$  is varied as  $\{60, 90, 120, 150, 180, 210\}$ . For individuals 7-9,  $\frac{N_{\text{test}}}{3}$  observations are created similarly, with  $N_{\text{test}} = 150$ .

We consider an additive GP model  $f = f^{(1)}(age) + f^{(2)}(age, z)$  with kernels

$$\begin{cases} k_1 &= \alpha_1^2 k_{\text{EQ}}(age, age' \mid \ell_1) \\ k_2 &= \alpha_2^2 k_{\text{ZS}}(z, z') k_{\text{EQ}}(age, age' \mid \ell_2) \end{cases} \quad (36)$$

and we simulate a realization of  $\mathbf{f} \in \mathbb{R}^{N_{\text{test}} + N_{\text{train}}}$  data using  $\alpha_1 = \alpha_2 = 1$ ,  $\ell_1 = 2$  and  $\ell_2 = 1$ . We then generate a response variable measurements  $\mathbf{y} = 100 + 10 \cdot (\mathbf{f} + \epsilon)$ , where  $\epsilon_i \sim \mathcal{N}(0, 0.5^2)$  and the realization  $\mathbf{f}$  represents the ground truth signal.

Data from individuals 1-6 is used in training, while data from individuals 7-9 is left for testing. Using the training data, we fit an exact and approximate model with the correct covariance structure from Eq. 36 using the Gaussian likelihood model. Exact model is fitted with `lgpr` (Timonen et al., 2021), which also uses Stan for MCMC. The exact model utilizes the marginalization approach for GPs (Sec. S3.2-S3.3), since Gaussian observation model is specified.

Fig. 1 shows the posterior predictive mean of the exact model and different approximate models with  $c = 1.5$ , using  $N_{\text{train}} = 150$ . We see that with  $B = 16$  and  $B = 32$  the mean predictions are indistinguishable from the exact model. We fit the approximate model using different values of  $B$  and  $c$ , and repeat the experiment using different values for  $N_{\text{train}}$ . Results in Fig. 3 validate empirically that the runtime scales linearly as a function of both  $N_{\text{train}}$  and  $B$ .



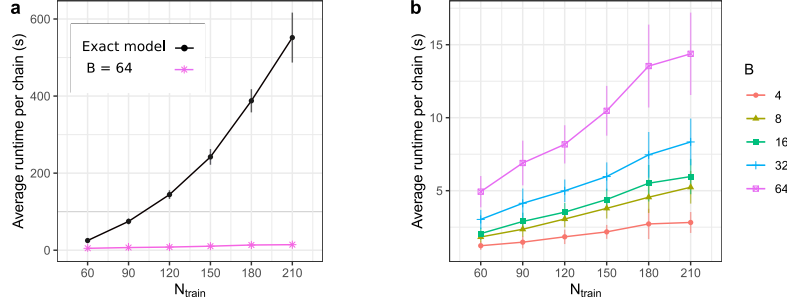


Figure 3: Runtimes of fitting the exact and approximate models in Experiment 1. **a)** Exact model vs. approximation with  $B = 64$ . **b)** Approximations using different values for  $B$ . The markers show the average time taken to run a chain, when a total of  $30 \times 4$  MCMC chains were run for 2000 iterations each. The vertical error bars show  $\pm$  one standard deviation (not shown for approximate model in panel **a**). Note the smaller y-axis scale in panel **b**. We see empirically that the runtime of the approximate model scales linearly in both  $N$  and  $B$ .

We compute the mean log predictive density (MLPD), at test points  $\mathbf{y}^* \in \mathbb{R}^{150}$  (see Sec. S3.1.2 for details about out-of-sample prediction and MLPD). Results in Fig. 2 show that the MLPD of the approximate model approaches the exact model as  $B$  grows. It is seen that with small data sizes and small  $B$ , the predictive performance can actually be better than that of the exact model, possibly because the coarser approximation is a simpler model that generalizes better in this case.

## 6.2 Experiment 2: Canadian weather data

We analyze data that consists of yearly average temperature measurements in 35 Canadian weather stations (Ramsay and Silverman, 2005). There is a total of  $N = 35 \times 365 = 12775$  data points, which are daily temperatures at the 35 locations, averaged over the years 1960-1994. We fit an additive GP model  $f = f^{(1)}(\text{day}) + f^{(2)}(\text{day}, \text{region}) + f^{(3)}(\text{day}, \text{station})$ , with Gaussian likelihood using the EQ kernel for  $f^{(1)}$  and the product EQ $\times$ ZS kernel for  $f^{(2)}$  and  $f^{(3)}$ .

We use domain scaling factor  $c = 1.5$  for all components and run 4 MCMC chains in parallel using 4 CPU cores on a cluster. This was repeated with different values of  $B = 8, 12, 16, 24, 32$ , where  $B$  is the number of basis functions for each component. Total runtimes for fitting the models were 4.10, 7.24, 7.47, 14.18 and 18.76 hours, respectively. The posterior distributions of each model component with  $B = 32$  are in Fig. 4. The posterior predictive distribution for each station separately is visualized in Fig. S1. Note that this data set with 12755 data points is large enough to make MCMC sampling for exact additive GP model fitting prohibitively slow.

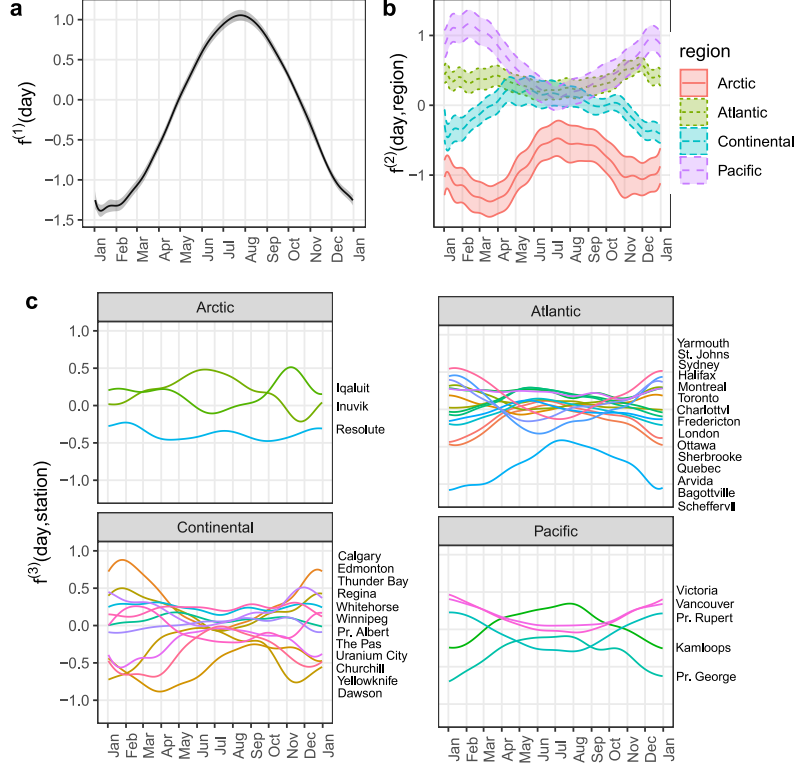


Figure 4: Results for the Canadian weather data experiment with  $B = 32$  and  $c = 1.5$ . Panels **a-c** show the marginal posterior distribution of each of the three components  $f^{(1)}$ ,  $f^{(2)}$  and  $f^{(3)}$  (mean  $\pm$  two times standard deviation). Standard deviation is not shown for  $f^{(3)}$  for clarity. The functions are on the standardized scale (response variable normalized to zero mean and unit variance). We see for example that the regions tend to have larger differences during winter. Notice that due to the specified categorical correlation structure, the effects of each region ( $f^{(2)}$ ) sum to zero at each time point, and so do also the effects specific to each station ( $f^{(3)}$ ). The sum-to-zero constraint disentangles the region or station specific time effects from the shared time effects.

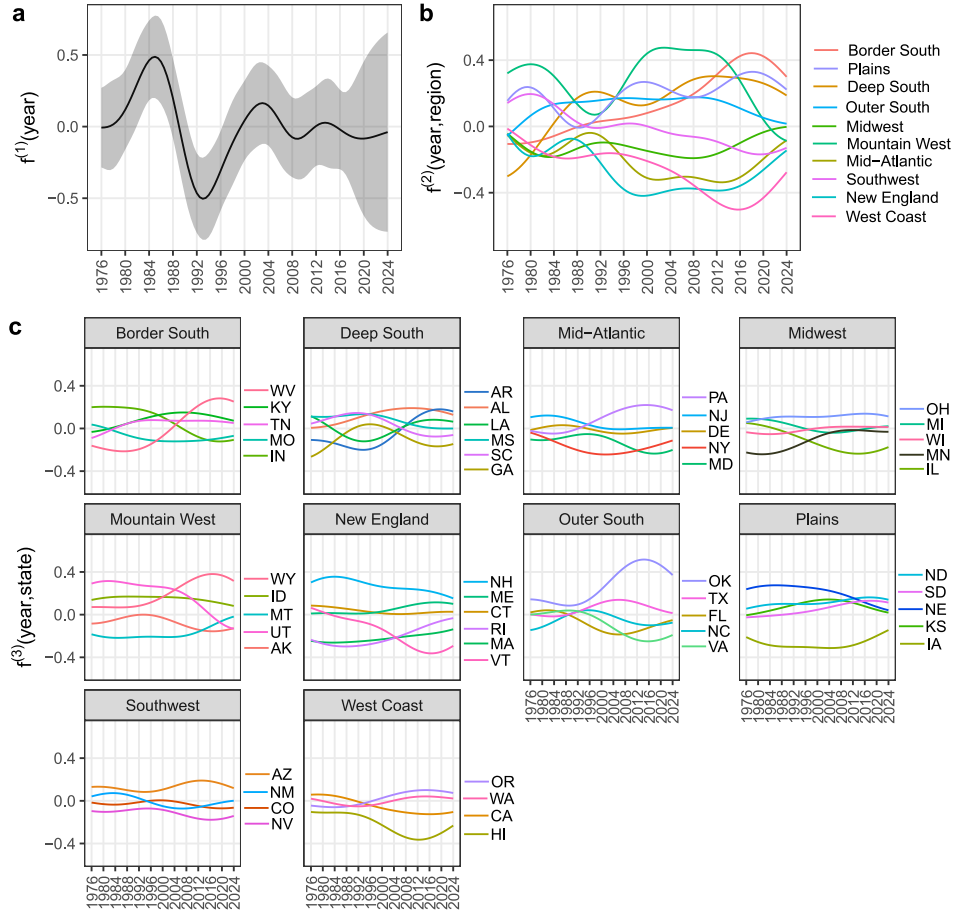


Figure 5: Results for the US election prediction experiment with  $B = 24$  and  $c = 2.0$ . Figures **a)**-**c)** show the marginal posterior distribution of each of the three components  $f^{(1)}$ ,  $f^{(2)}$  and  $f^{(3)}$  (mean  $\pm$  two times standard deviation). Standard deviation is not shown for  $f^{(2)}$  and  $f^{(3)}$  for clarity.

### 6.3 Experiment 3: US presidential election prediction

In this example we demonstrate a beta-binomial observation model and model the vote share of the Republican Party in each state in US presidential elections. By two-party vote share we mean proportion of votes cast to the Republican candidate divided by the sum of votes to both the Republican and Democratic candidates<sup>4</sup>. Following [Trangucci \(2017\)](#), Washington DC is excluded from the analysis. We use data from the 1976-2016 elections as training data, meaning that  $N = 50 \times 11 = 550$ .

We fit an additive GP model  $f = f^{(1)}(year) + f^{(2)}(year, region) + f^{(3)}(year, state)$ , with beta-binomial observation model using the EQ kernel for  $f^{(1)}$  and the product EQ $\times$ ZS kernel for  $f^{(2)}$  and  $f^{(3)}$ . The observation model is

$$y^R \sim \text{Beta-Binomial}(y^R + y^D, a, b), \quad (37)$$

where  $y^R, y^D$  are the number of votes for the Republican and Democratic parties, respectively,  $a = \rho(\gamma^{-1} - 1)$ ,  $b = (1 - \rho)(\gamma^{-1} - 1)$ , and  $\rho = \text{inv-logit}(f + w_0)$ . We use a  $\mathcal{N}(0, 0.5^2)$  prior for the intercept  $w_0$  and a Log-Normal(1,1) prior for the  $\gamma$  parameter.

The posterior distributions of each model component are in Fig. 5. See also Fig. S2, where we have also visualized the data from 2020 election to validate that the model predicts well into the future. Fitting a model with  $B = 24$  and  $c = 2.0$  on a laptop computer<sup>5</sup> running 4 MCMC chains in parallel took approximately 18 minutes. It is possible to fit an exact GP model to a dataset of this size, but we estimate it would take more than a day on the same machine.

### 6.4 Experiment 4: Model reduction with simulated data

We use the `lgpr` package to simulate data from an additive GP model with a shared *age* effect (nonlinear), *id*-specific effect (baseline offset), a category-specific effect of a 2-level categorical variable *z* (nonlinear), a category-specific effect of a 3-level categorical variable *r* (nonlinear), a shared effect of a continuous variable *x* (nearly linear), and a shared effect of a continuous variable *w* (nearly linear). Furthermore, we add  $U = 16$  continuous nuisance variables  $x_1, \dots, x_U$  and  $U = 16$  2-level categorical nuisance variables  $z_1, \dots, z_U$ . While  $x, w$  are generated independently, the continuous nuisance variables are drawn from a multivariate Gaussian distribution so that their correlation with  $x$  is  $\rho = 0.85$ . The categorical nuisance variables are created from  $z$  so that their category is flipped for  $\frac{1}{3}$  of the individuals, in order to induce correlation also between the categorical variables and thus make the model reduction task more difficult. The number of individuals is 50, and with 16 observations each, the data set size is  $N = 800$ .

The signal in the true model to generate data is

$$f_{\text{true}} = f^{(1)}(id) + f^{(2)}(age) + f^{(3)}(age, z) + f^{(4)}(age, r) + f^{(5)}(x) + f^{(6)}(w) \quad (38)$$

<sup>4</sup>Data is from ([MIT Election Data and Science Lab, 2017](#)).

<sup>5</sup>2018 MacBook Pro, 3 GHz Quad-Core Intel i5 CPU

and Gaussian noise is added so that signal-to-noise ratio is  $\text{SNR} = \{0.1, 0.25, 0.5\}$ . The fitted reference model  $\mathcal{M}_{\text{ref}}$  is

$$f_{\text{ref}} = f_{\text{true}} + \sum_{u=1}^U f_x^{(u)}(x) + \sum_{u=1}^U f_z^{(u)}(\text{age}, z_u) \quad (39)$$

and we use the EQ kernel to model the shared effects and the EQ $\times$ ZS product kernel for category-specific *age* effects, while the effect of *id* is a subject-specific offset. The total number of terms is therefore  $6 + 2U = 38$ . We compare methods to reduce this model to the simplest possible, i.e. ideally the one with the "true" relevant covariates *id*, *age*, *x*, *z*, *w*, *r*, or a small model with equal predictive performance. When performing a forward search, we always assume that  $f^{(1)}(\text{id})$  and  $f^{(2)}(\text{age})$  are in the model due to their special nature in longitudinal modeling. Additional details on the experiment setup are in Sec. S1.2.

We compare two search heuristics for the projection predictive method; a greedy forward search based on KL divergence against the reference model, and a pre-specified search path given by the component relevances determined via the additive variance decomposition (AVD, Sec. 5.1). To speed up the search, we project only a subsample of 30 posterior draws during forward search, and rank the submodels based on the mean pointwise KL divergence between the projected predictive distribution of the submodel and reference model. After every forward search step  $k$ , we project 100 draws to compute the expected projected log predictive density (ELPD) estimate  $\hat{u}_k$  for the chosen submodel, approximated using Pareto-smoothed importance sampling leave-one-out cross validation (PSIS-LOO) (Vehtari et al., 2017). ELPD for the reference model,  $\hat{u}^*$ , is computed using PSIS-LOO with all posterior draws. Both stepwise methods are run until the model has  $k = 8$  terms.

Fig. 6a shows, as a function of model size  $k$ , the estimated relative difference in ELPD (Eq. 28). We see that the difference between the two search heuristics is very small, but the forward search can achieve a slightly better ELPD on average at given  $k$ . With  $\text{SNR} = 0.1$ , the data is so noisy that already the empty model has similar predictive performance as the reference model. With  $\text{SNR} = 0.25$ , three terms are usually required and with  $\text{SNR} = 0.5$ , five to six terms are required.

In Fig. 6b, we provide as comparison the cumulative relevance (Eq. 27) given by AVD at each step  $k$ , using the same two search heuristics for the submodel. Plotted with the black horizontal dashed line is a possible threshold 0.95, used in Timonen et al. (2021), which seems to result in larger model sizes than projection predictive method, difference being clearest in the  $\text{SNR} = 0.1$  case where three to four variables are usually needed.

In Fig. 6c, we compare the proportion of "true" terms in the model by each method at each step of the search path. The forward search path seems to perform better choices on average. To shed light on the types of wrong selections, we plot the distribution of the selected term at steps  $k = 3, 4, 5, 6$  (i.e. after the *id* and *age* terms that are fixed in the model at  $k = 1, 2$ ) in Fig. S3. We see for example that selecting categorical nuisance variables into the model is more common than selecting continuous nuisance variables in this experiment.

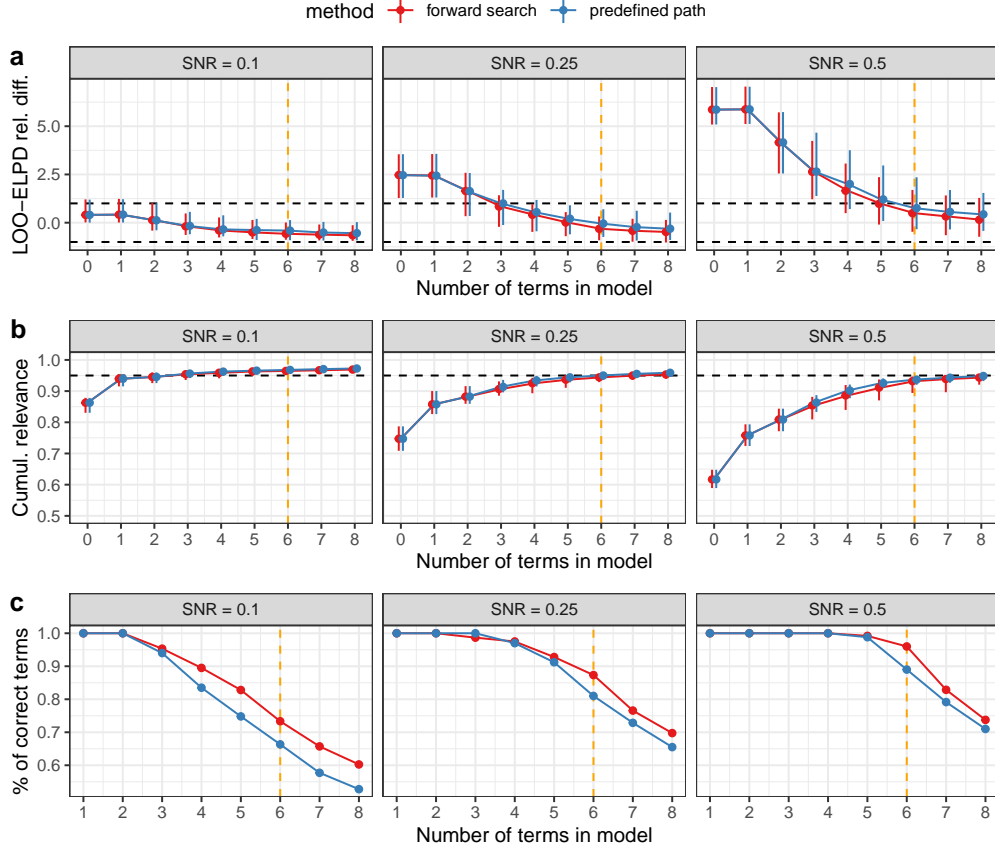


Figure 6: Model reduction comparison experiment, with different values for the signal-to-noise ratio  $\text{SNR} = \{0.1, 0.25, 0.5\}$ . The orange dashed vertical line shows the true model size used to generate the data. **a)** The estimated relative difference  $\Delta_{\text{ELPD}}^k$  in predictive performance (lower is better) shows that the greedy forward search is able to find on average slightly better models with a given number of variables  $k$  than the predefined path based on the componentwise relevances obtained via the additive variance decomposition (AVD). The black horizontal dashed lines represent the model size selection rule  $|\Delta_{\text{ELPD}}^k| \leq 1$ , and we see that the model size needed to satisfy it depends on the SNR. **b)** Cumulative relevance (explained variation) of the submodel with a given number of terms, given by AVD. The black horizontal dashed lines represent the model size selection threshold 0.95, and we see that the model size needed to satisfy it also depends on the SNR. The dots in panels **a-b** show the median and the error bars show 90% central credible intervals over the 50 repetitions. **c)** Proportion of “true” terms in the model at each step of the model search path. Shown are averages over the 50 repeated simulation experiments.

In Table S1, we report the average runtimes for different parts of performing the model reduction workflow. We see that running the full forward search for 8 steps takes a similar amount of time as fitting the reference model, and the search using the predefined search path based on AVD takes an order of magnitude less time, as computing the AVD has a negligible runtime. We note that in practice the search would be stopped as the stopping condition for model size is met, which usually occurs earlier.

An additional experiment with a larger data set and different number of true variables is described in Sec. S2.1.

## 7 Limitations

The approximation method that we use requires that the continuous kernels are stationary. Non-stationary effects can still be modeled by applying a warping on the input first, and then using a stationary kernel (see for example Snoek et al. (2014)). Another limitation is that we use kernels that are composed of sums and products of base kernels. It is possible to construct a mixed-domain kernel that does not fit into this family, as is done in Sec. S2.2, where we study one such kernel. However, we find this example rather artificial, and in reality additive kernels with low-dimensional base kernels have demonstrated good predictive performance (Lu et al., 2022), and have the advantage of increased model interpretability.

In Sec. 6, the largest data size that was analyzed was  $N = 12775$  observations. In Sec. S2.3, we push the modeling framework further to study the practical scalability limit. We find estimate that with our implementation, it is viable to analyze data sets on the order of  $N = 10^5$  when the total number of basis functions  $M$  is on the order of hundreds (see Sec. 4.1). This practical limit arises largely due to using full Bayesian inference with MCMC, as Stan does not scale well to millions of observations.

## 8 Conclusion

Gaussian processes offer an attractive framework for specifying flexible models using a kernel language. The computational cost of their exact inference however limits possible applications to small data sets, and the complexity of alternative model spaces poses additional limits for the scalability of a useful model building workflow. Our scalable framework opens up a rich class of GP models to be used in large scale applications of various fields of science as the computational complexity is linear with respect to data size. We have presented a scalable approximation scheme for mixed-domain covariance functions, and demonstrated its use in the context of Bayesian GP regression. However, it can also be applied in GP applications where the kernel hyperparameters are optimized using a marginal likelihood criterion.

Based on the model reduction experiments, the projection based full forward search seems to be able to rank the variables in a better order based on whether they were actually in the data-generating model. However, we note that the practical relevance of the "false" variables that are correlated with the "true" variables is not zero since they

retain some of predictive information of the "true" variables. The additive variance decomposition (AVD) method seems to perform remarkably well in selecting small models that have a good predictive performance even in challenging settings and in the presence of a multitude of collinear predictors. It is a viable candidate for ranking the variables in applications where performing a full forward search is prohibitively slow due to the larger number of alternative models at each step, and also useful for determining the final model size. One reason for why the AVD works well for these longitudinal models is the fact that in the full model we use the zero-sum categorical kernel in interaction terms with age to disentangle the effect of the categorical variable on the explained variance from that of the shared effect of age.

Note that in the model reduction experiments we used approximate estimation of the ELPD and did not test the performance on actual hold out data. In practice it is important to interpret the projected posterior as explained in [McLatchie et al. \(2024\)](#), to assess whether it can actually be used for out-of-sample prediction in addition to just model ranking during the model space search. A safe alternative is to refit the final found submodel using its own posterior instead of the projected posterior for final evaluation or prediction. In addition, it can be useful to diagnose the model search path using cross-validation over the entire model search if signs of over-optimism are detected ([McLatchie et al., 2024](#)). One sign is the ELPD of the submodel exceeding the ELPD of the reference model, which we did not see in our experiments, and therefore did not cross-validate the search path due to increased computational demands. The final model size determination is always inherently dependent on some threshold rule and setting the optimal threshold depends on factors such as the amount of noise in the data, as seen in our experiments (see also Sec. S2). For the models discussed in this paper, it seems beneficial to look at both the relative difference in ELPD and cumulative relevance, and whether these metrics plateau rather than whether they exceed a given threshold.

### Acknowledgments

We thank Aki Vehtari and Gleb Tikhonov for useful comments on early versions of this manuscript, and acknowledge the computational resources provided by Aalto Science-IT, Finland. We wish to also thank anonymous reviewers for their constructive comments.

### Funding

This work was supported by the Academy of Finland and Bayer Oy.

## Supplementary Material

Scalable mixed-domain Gaussian process modeling and model reduction for longitudinal data: Supplementary material. Sections S1-S3, Figures S1-S7, Table S1.



## References

- Cao, Y., Brubaker, M. A., Fleet, D. J., and Hertzmann, A. (2015). “Efficient Optimization for Sparse Gaussian Process Regression.” *IEEE Transactions on Pattern Analysis and Machine Intelligence*, 37(12): 2415–2427. [6](#)
- Carpenter, B., Gelman, A., Hoffman, M. D., Lee, D., Goodrich, B., Betancourt, M., Brubaker, M., Guo, J., Li, P., and Riddell, A. (2017). “Stan: A Probabilistic Programming Language.” *Journal of Statistical Software*, 76(1): 1–32. [14](#)
- Catalina, A., Bürkner, P.-C., and Vehtari, A. (2022). “Projection Predictive Inference for Generalized Linear and Additive Multilevel Models.” In *Proceedings of The 25th International Conference on Artificial Intelligence and Statistics*. [12](#), [13](#)
- Chambers, J. M. and Hastie, T. J. (1992). *Statistical Models in S*. London: Chapman & Hall, 1st edition. [9](#)
- Cheng, L., Ramchandran, S., Vatanen, T., Lietzen, N., Lahesmaa, R., Vehtari, A., and Lähdesmäki, H. (2019). “An additive Gaussian process regression model for interpretable non-parametric analysis of longitudinal data.” *Nature Communications*, 10. [1](#), [2](#), [5](#), [11](#)
- Chung, I., Kim, S., Lee, J., Kim, K. J., Hwang, S. J., and Yang, E. (2020). “Deep Mixed Effect Model using Gaussian Processes: A Personalized and Reliable Prediction for Healthcare.” *The Thirty-Fourth AAAI Conference on Artificial Intelligence (AAAI-20)*. [6](#)
- Deng, X., Lin, C. D., Liu, K.-W., and Rowe, R. K. (2017). “Additive Gaussian Process for Computer Models With Qualitative and Quantitative Factors.” *Technometrics*, 59(3): 283–292. [1](#)
- Fortuin, V., Dresdner, G., Strathmann, H., and Rätsch, G. (2021). “Sparse Gaussian Processes on Discrete Domains.” *IEEE Access*, 9: 76750–76758. [6](#)
- Garrido-Merchán, E. C. and Hernández-Lobato, D. (2020). “Dealing with categorical and integer-valued variables in Bayesian Optimization with Gaussian processes.” *Neurocomputing*, 380: 20–35. [1](#), [5](#)
- Gelman, A., Goodrich, B., Gabry, J., and Vehtari, A. (2019). “R-squared for Bayesian regression models.” *The American Statistician*, 73(3): 307–309. [11](#)
- Goutis, C. and Robert, C. P. (1998). “Model choice in generalised linear models: A Bayesian approach via Kullback-Leibler projections.” *Biometrika*, 85(1): 29–37. [12](#)
- Kaufman, C. G. and Sain, S. R. (2010). “Bayesian functional ANOVA modeling using Gaussian process prior distributions.” *Bayesian Analysis*, 5(1): 123–149. [5](#)
- Kimeldorf, G. S. and Wahba, G. (1970). “A Correspondence Between Bayesian Estimation on Stochastic Processes and Smoothing by Splines.” *The Annals of Mathematical Statistics*, 41(2): 495 – 502. [6](#)
- Liu, H., Ong, Y.-S., Shen, X., and Cai, J. (2020). “When Gaussian Process Meets

- Big Data: A Review of Scalable GPs.” *IEEE Transactions on Neural Networks and Learning Systems*, 31(11): 4405–4423. 2
- Lu, X., Boukouvalas, A., and Hensman, J. (2022). “Additive Gaussian Processes Revisited.” In Chaudhuri, K., Jegelka, S., Song, L., Szepesvari, C., Niu, G., and Sabato, S. (eds.), *Proceedings of the 39th International Conference on Machine Learning*, volume 162 of *Proceedings of Machine Learning Research*, 14358–14383. PMLR. 23
- McLatchie, Y., Rögnvaldsson, S., Weber, F., and Vehtari, A. (2024). “Advances in projection predictive inference.”  
URL <https://arxiv.org/abs/2306.15581> 12, 24
- MIT Election Data and Science Lab (2017). “U.S. President 1976–2020, V6.” 20
- Pavone, F., Piironen, J., Burkner, P.-C., and Vehtari, A. (2020). “Using reference models in variable selection.” *Computational Statistics*, 38: 349–371. 2, 11, 12
- Pedersen, E., Miller, D., Simpson, G., and Ross, N. (2019). “Hierarchical generalized additive models in ecology: An introduction with mgcv.” *PeerJ*, (5). 6
- Piironen, J., Paasiniemi, M., and Vehtari, A. (2020). “Projective inference in high-dimensional problems: Prediction and feature selection.” *Electronic Journal of Statistics*, 14(1): 2155 – 2197. 12
- Piironen, J. and Vehtari, A. (2017). “Comparison of Bayesian predictive methods for model selection.” *Statistics and Computing*, 27(3): 711–735. 12
- Pinheiro, J. C. and Bates, D. M. (2000). *Mixed-effects models in S and S-PLUS*. New York, NY: Springer. 9
- Qian, P. Z. G., Wu, H., and Wu, C. F. J. (2008). “Gaussian Process Models for Computer Experiments With Qualitative and Quantitative Factors.” *Technometrics*, 50(3): 383–396. 1, 6
- Quiñonero Candela, J. and Rasmussen, C. E. (2005). “A Unifying View of Sparse Approximate Gaussian Process Regression.” *J. Mach. Learn. Res.*, 6: 1939–1959. 6
- Quintana, F. A., Johnson, W. O., Waetjen, L. E., and Gold, E. B. (2016). “Bayesian Nonparametric Longitudinal Data Analysis.” *Journal of the American Statistical Association*, 111(515): 1168–1181. 5
- R Core Team (2023). *R: A Language and Environment for Statistical Computing*. R Foundation for Statistical Computing, Vienna, Austria.  
URL <https://www.R-project.org/> 2
- Ramsay, J. and Silverman, B. W. (2005). *Functional Data Analysis*. Springer, New York, NY, 2nd edition. 17
- Rasmussen, C. E. and Williams, C. K. I. (2006). *Gaussian Processes for Machine Learning*. Cambridge, Massachusetts: MIT Press. 3, 10
- Riutort-Mayol, G., Bürkner, P.-C., Andersen, M. R., Solin, A., and Vehtari, A. (2022). “Practical Hilbert space approximate Bayesian Gaussian processes for probabilistic programming.” *Statistics and Computing*, 33(1). 6, 14

- Roustant, O., Padonou, E., Deville, Y., Clément, A., Perrin, G., Giorla, J., and Wynn, H. (2020). “Group Kernels for Gaussian Process Metamodels with Categorical Inputs.” *SIAM/ASA Journal on Uncertainty Quantification*, 8(2): 775–806. 1, 6, 9
- Sacks, J., Welch, W. J., Mitchell, T. J., and Wynn, H. P. (1989). “Design and Analysis of Computer Experiments.” *Statistical Science*, 4(4): 409–423. 6
- Shmueli, G. (2010). “To Explain or to Predict?” *Statistical Science*, 25(3): 289 – 310. 11
- Snelson, E. and Ghahramani, Z. (2006). “Sparse Gaussian Processes using Pseudo-inputs.” In *Advances in Neural Information Processing Systems*, volume 18. 2
- Snoek, J., Swersky, K., Zemel, R., and Adams, R. P. (2014). “Input warping for Bayesian optimization of non-stationary functions.” In *Proceedings of the 31st International Conference on International Conference on Machine Learning*, volume 32. 23
- Solin, A. and Särkkä, S. (2020). “Hilbert space methods for reduced-rank Gaussian process regression.” *Statistics and Computing*, 30: 419–446. 2, 6, 7, 8
- Timonen, J., Mannerström, H., Vehtari, A., and Lähdesmäki, H. (2021). “lgpr: an interpretable non-parametric method for inferring covariate effects from longitudinal data.” *Bioinformatics*, 37(13): 1860–1867. 1, 2, 5, 11, 14, 16, 21
- Titsias, M. (2009). “Variational Learning of Inducing Variables in Sparse Gaussian Processes.” In *Proceedings of the 12th International Conference on Artificial Intelligence and Statistics*, volume 5. 2
- Trangucci, R. (2017). “Hierarchical Gaussian Processes in Stan.”  
URL <https://mc-stan.org/events/stancon2017-notebooks/stancon2017-trangucci-hierarchical-gps.pdf> 20
- Vehtari, A., Gelman, A., and Gabry, J. (2017). “Practical Bayesian model evaluation using leave-one-out cross-validation and WAIC.” *Statistics and Computing*, 27(5): 1413–1432. 21
- Verbeke, G. and Molenberghs, G. (2000). *Linear Mixed Models for Longitudinal Data*. Springer, New York, NY. 5
- Wang, L., Yerramilli, S., Iyer, A., Apley, D., Zhu, P., and Chen, W. (2021). “Scalable Gaussian Processes for Data-Driven Design Using Big Data With Categorical Factors.” *Journal of Mechanical Design*, 144(2). 1
- Wilson, A. G. and Nickisch, H. (2015). “Kernel interpolation for scalable structured Gaussian processes (KISS-GP).” In *Proceedings of the 32nd International Conference on International Conference on Machine Learning*, volume 37. 2
- Wood, S. (2017). *Generalized Additive Models: An Introduction with R*. Chapman and Hall/CRC, 2nd edition. 13
- Zhang, Y. and Notz, W. I. (2015). “Computer Experiments with Qualitative and Quantitative Variables: A Review and Reexamination.” *Quality Engineering*, 27: 2–13. 1

Zhang, Y., Tao, S., Chen, W., and Apley, D. W. (2020). “A Latent Variable Approach to Gaussian Process Modeling with Qualitative and Quantitative Factors.” *Technometrics*, 62(3): 291–302. [6](#)

# Scalable mixed-domain Gaussian process modeling and model reduction for longitudinal data: Supplementary material

Juho Timonen<sup>1</sup> and Harri Lähdesmäki<sup>1</sup>

<sup>1</sup>Aalto University, Department of Computer Science

March 12, 2025

## Contents

<b>S1 Experiment details</b>	<b>1</b>
S1.1 Scalability experiments . . . . .	1
S1.2 Model reduction experiments . . . . .	4
<b>S2 Supplementary experiments</b>	<b>6</b>
S2.1 Model reduction . . . . .	6
S2.2 Model mismatch . . . . .	6
S2.3 Practical scalability limit . . . . .	9
<b>S3 Supplementary methods</b>	<b>11</b>
S3.1 Approximate posterior predictive distribution . . . . .	11
S3.1.1 Componentwise approximate posteriors of additive GPs . . . . .	11
S3.1.2 Mean log predictive density . . . . .	11
S3.2 Exact GP regression under Gaussian observation model . . . . .	11
S3.2.1 Model inference . . . . .	11
S3.2.2 Prediction . . . . .	12
S3.3 Approximate GP regression with $\mathbf{f}$ marginalized out . . . . .	12
S3.4 Derivation of Equation 35 of main text . . . . .	13
S3.5 Practical considerations . . . . .	13
S3.6 Multivariate normal distribution . . . . .	13
S3.7 Matrix identities . . . . .	13

## S1 Experiment details

This section describes the experiments presented in the main manuscript in more detail.

### S1.1 Scalability experiments

Experiments 1-2 and were run on a modern CentOS 7 computing cluster and Experiment 3 on a laptop computer. Version 2.27 of Stan ([Carpenter et al., 2017](#)) was used with the Dynamic HMC algorithm with target acceptance rate set to 0.95, for MCMC sampling the parameters of our approximate

models. Models were fitted by running four independent MCMC chains for 2000 iterations each, discarding the first half of each chain as warmup. We used Student- $t$  priors with 20 degrees of freedom for the  $\alpha$  kernel parameters and log-normal priors with mean 0 and scale 1 for kernel lengthscale parameters  $\ell$ . In Experiments 1 and 2 the noise variance parameter  $\sigma^2$  of the Gaussian observation model has an Inverse-Gamma prior with shape parameters  $\alpha = 1$  and  $\beta = 2$ . Priors are on normalized data scale, meaning that continuous variables are standardized to zero mean and unit variance during inference.

Mean log predictive density was computed as explained in Section S3.1.2.

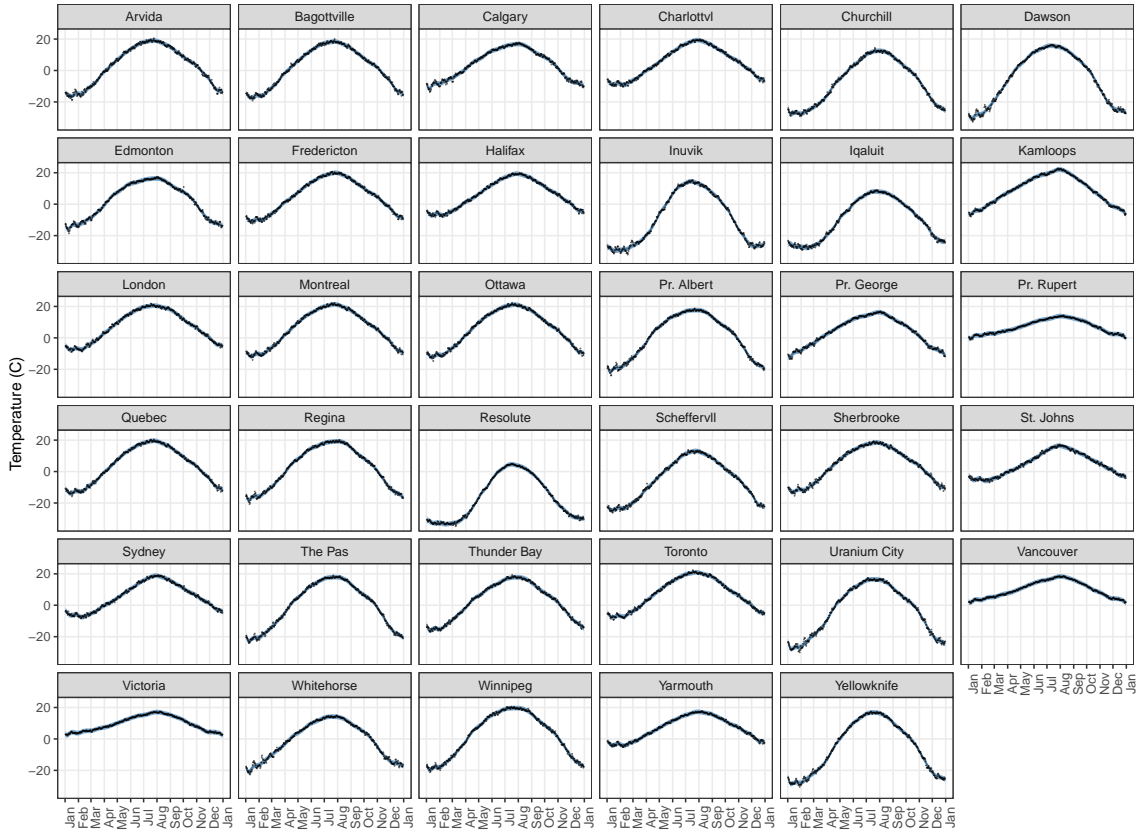


Figure S1: Results for the Canadian weather data experiment with  $B = 32$  and  $c = 1.5$ . Figure shows the posterior predictive distribution for new observations. The dark blue line is the mean and the shaded ribbon extends to mean  $\pm$  two times standard deviation. Black dots are data. Results for the corresponding exact GP model are not shown as comparison as fitting the exact model was virtually not possible (due to large amount of data and cubic scaling). In this application the observation time points happen to be equally spaced and same for all observation units (stations), but our approximation method does not require this to be the case.

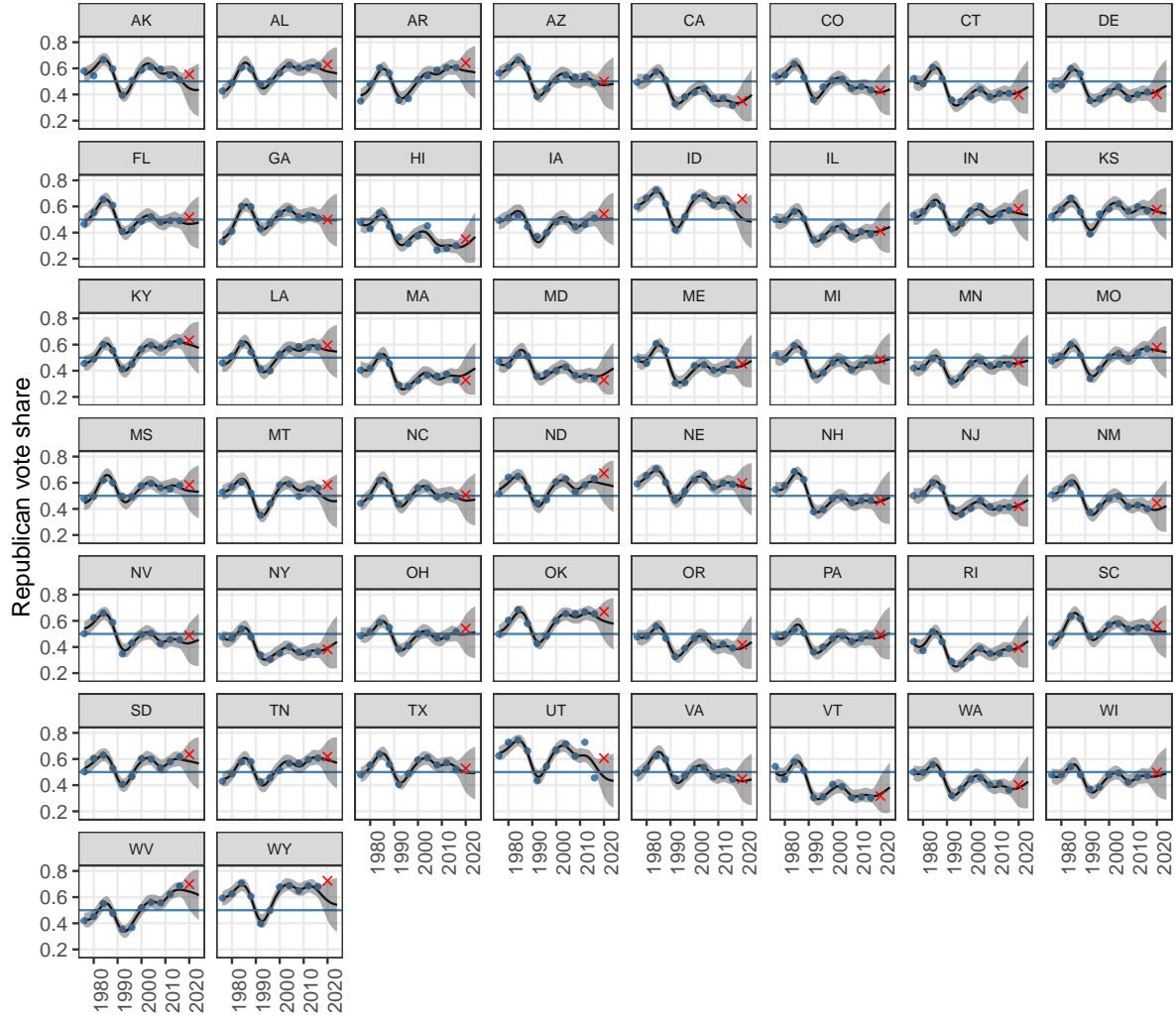


Figure S2: Results for the election prediction experiment. Figure shows the posterior predictive distribution of the Republican vote share for each state, for years 1976-2024. The black line is the mean and the shaded ribbon extends to mean  $\pm$  two times standard deviation). Data from years 1976-2016 were used as training data (blue dots) and year 2020 is shown as test data (red crosses).

## S1.2 Model reduction experiments

The experiments were run on a modern CentOS 7 computing cluster using version 2.32 of Stan and the development version 0.0.3 of `lgpr2`. For fitting the reference models, the Dynamic HMC algorithm of Stan was used with target acceptance rate set to 0.99. The reference models were fitted by running two independent MCMC chains for 2000 iterations each, discarding the first half of each chain as warmup. We used the same number of basis functions  $B = 24$  and domain scaling factor  $c = 1.5$  for each approximate continuous kernel. We used the same priors for the kernel hyperparameters as in the scalability experiments, except for a  $\text{LogNormal}(1,1)$  prior for the noise standard deviation  $\sigma$ .

The simulated longitudinal data was generated using the `simulate.data()` function in the `lgpr` package version 1.2.4 (Timonen et al., 2021). The observation time points for each subject were at ages 6–96 months at 6-month intervals, with small subject-specific jitter added to the observation times. Other true continuous covariates were drawn from the standard normal distribution. The true non-linear effects were generated from (group-specific) Gaussian processes using lengthscale 12. This made the effects of continuous variables other than age nearly linear, while the shared age and group-specific age effects were highly nonlinear.

Setup	SNR = 0.1	SNR = 0.25	SNR = 0.5
mean_mcmc_time	2102.1	2442.0	2904.8
mean_forward_search_time	1975.9	1627.9	1422.7
mean_predefined_path_time	169.1	135.7	113.0
mean_num_divergent	0	0	0
mean_num_max_treedepth	0	0	0
mean_max_rhat	1.012	1.013	1.014
sd_max_rhat	0.003	0.002	0.004
max_max_rhat	1.023	1.020	1.029

Table S1: Runtimes and diagnostics in the main model reduction experiment with different signal-to-noise ratios (SNR). The reported times are in seconds. The remaining rows are MCMC sampler performance and convergence diagnostics (Stan Development Team, 2024). We see that fitting the full reference model (`mean_mcmc_time`) is the most time consuming part in this setup. No sampling problems are detected and convergence is satisfactory.



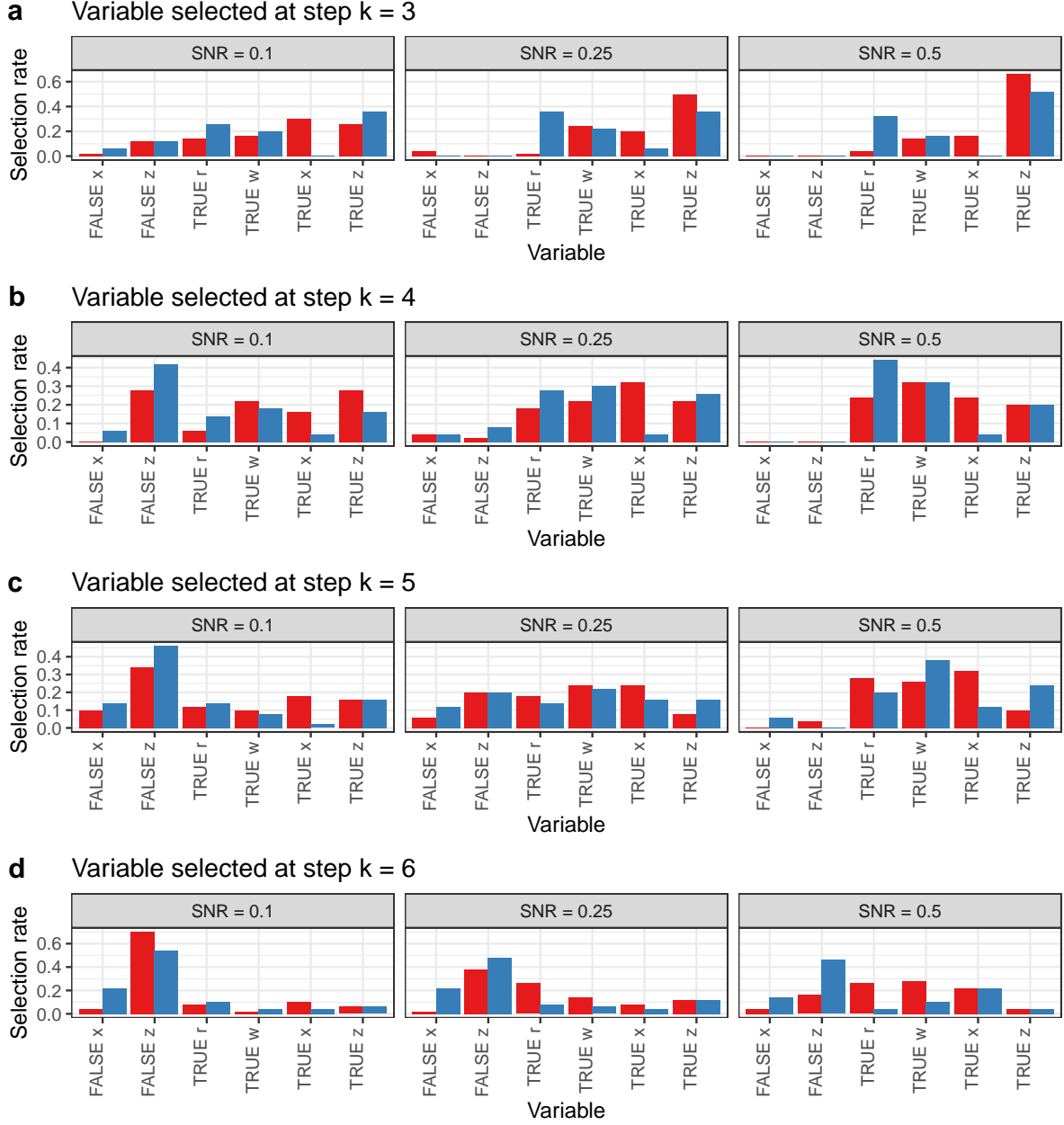


Figure S3: Variable selection accuracy in the model reduction experiment with different signal-to-noise ratios (SNR). **a-d**) Selection rate (proportion of times a given variable is selected) of each variable or variable type at step  $k$ , after the steps  $k = 1, 2$  that always correspond to the special baseline variables *id* and *age*, respectively. The red bars show the results for the greedy forward search, and blue bars for the predefined search path using ranking based on component relevances obtained via an additive variance decomposition. We see for example that selecting false categorical variables  $z$  is more common than false continuous variables  $x$  in this experiment setup.

## S2 Supplementary experiments

In this section we provide additional experiments not presented in the main manuscript.

### S2.1 Model reduction

We repeat the model reduction experiment of the main manuscript with otherwise the same details but increase the number of subjects to 100, for a total data size of  $N = 1600$ . This likely makes the true effects more easily identifiable. We also remove the variables  $w$  and  $r$  from the analysis, so that the true model size is 4. We run the search paths until  $k = 6$  variables.

The results are shown in Figure S4 and Figure S5, similarly as for the main model reduction experiment. We see that it is possible that the submodel performance plateaus before reaching a value close enough to the reference model performance (Figure S4c with SNR = 0.5). This can be due to the fact that we have used as  $s_k^*$  the estimated standard error of the reference model ELPD, and not the standard error of the difference  $\hat{u}^* - \hat{u}_k$ . The latter would be nontrivial to assess in our case, since we have used all posterior MCMC draws for estimating the reference model utility and only a subset for the submodel ELPD due to scalability reasons.

Here the model size selection rule based on cumulative relevance works better as it on average selects the correct model size  $k = 4$ . However, it may be best to look at both the relative difference in ELPD and cumulative relevance, and whether they plateau rather than whether they exceed a given threshold, since setting such threshold is not easy to do in a widely applicable manner.

### S2.2 Model mismatch

In order to clarify the limitations of our framework, we demonstrate a case of model mismatch where the data is generated using a kernel constructed so that it does not fit into our approximation scheme. It involves a categorical group indicator variable  $z \in \{1, 2, 3\}$  and a continuous variable  $x$ , and is defined as

$$k_{\text{TRUE}}((x, z), (x', z')) = \exp\left(-\frac{1}{2}\left(\frac{x}{\ell(z)} - \frac{x'}{\ell(z')}\right)^2\right), \quad (1)$$

where  $\ell(1) = 1$ ,  $\ell(2) = 0.5$ , and  $\ell(3) = 0.2$ . This kernel is not separable and cannot be written using just products and sums of base kernels for  $x$  and  $z$ .

Values for  $x$  are generated roughly uniformly on the interval  $[-1, 1]$ . Each group  $z$  has the same number of observations. The generated signal is drawn from the Gaussian process with kernel  $k_{\text{TRUE}}$  and Gaussian noise with variance  $\sigma_{\text{TRUE}}^2$  is added to it to create noisy observations. We leave observations that satisfy  $-0.3 < x < 0.5$  and  $z \in 2, 3$  as test points, the remaining ones being training data.

We try to fit approximate GP models with Gaussian observation model, using two kernels that fit into our approximation scheme. These are

- $k_A((x, z), (x', z')) = k_{\text{ZS}}(z, z') \cdot k_{\text{EQ}}(x, x' \mid \alpha, \ell)$
- $k_B((x, z), (x', z')) = k_{\text{ZS}}(z, z') \cdot k_{\text{EQ}}(x, x' \mid \alpha_1, \ell_1) + k_{\text{EQ}}(x, x' \mid \alpha_2, \ell_2)$ .

The kernel  $k_A$  is separable because it can be written as a product of kernels for  $x$  and  $z$ . The kernel  $k_B$  adds the shared effect of  $x$  into this. The models were fit using the `lgpr2` package<sup>1</sup> with

- `k_A : modelA <- LonModel$new(y ~ gp(x, z))`
- `k_B : modelB <- LonModel$new(y ~ gp(x, z) + gp(x))`

---

<sup>1</sup>version 0.0.3

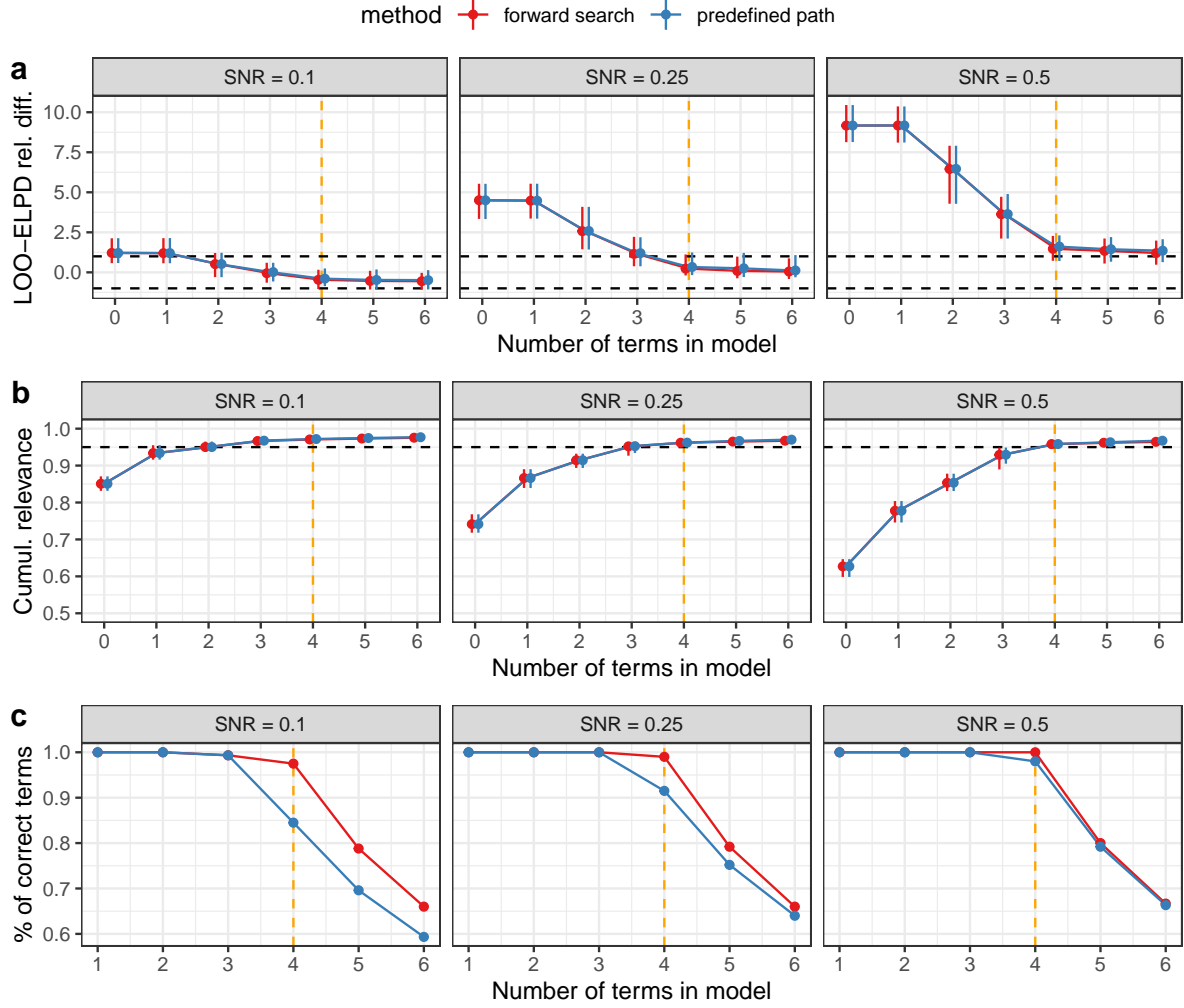


Figure S4: Supplementary model reduction comparison experiment, with 50 repeated simulations in each case  $\text{SNR} = \{0.1, 0.25, 0.5\}$ . The dashed orange vertical line shows the true model size used to generate the data. **a**) Mean relative difference in ELPD (approximated using PSIS-LOO) compared to reference model over the 50 repetitions. **b**) Cumulative relevance (explained variation) of the submodel with a given number of terms. The dots show the median and the error bars show 90% central intervals over the 50 repetitions. **c**) Proportion of correct terms in the model at each step  $k$ .

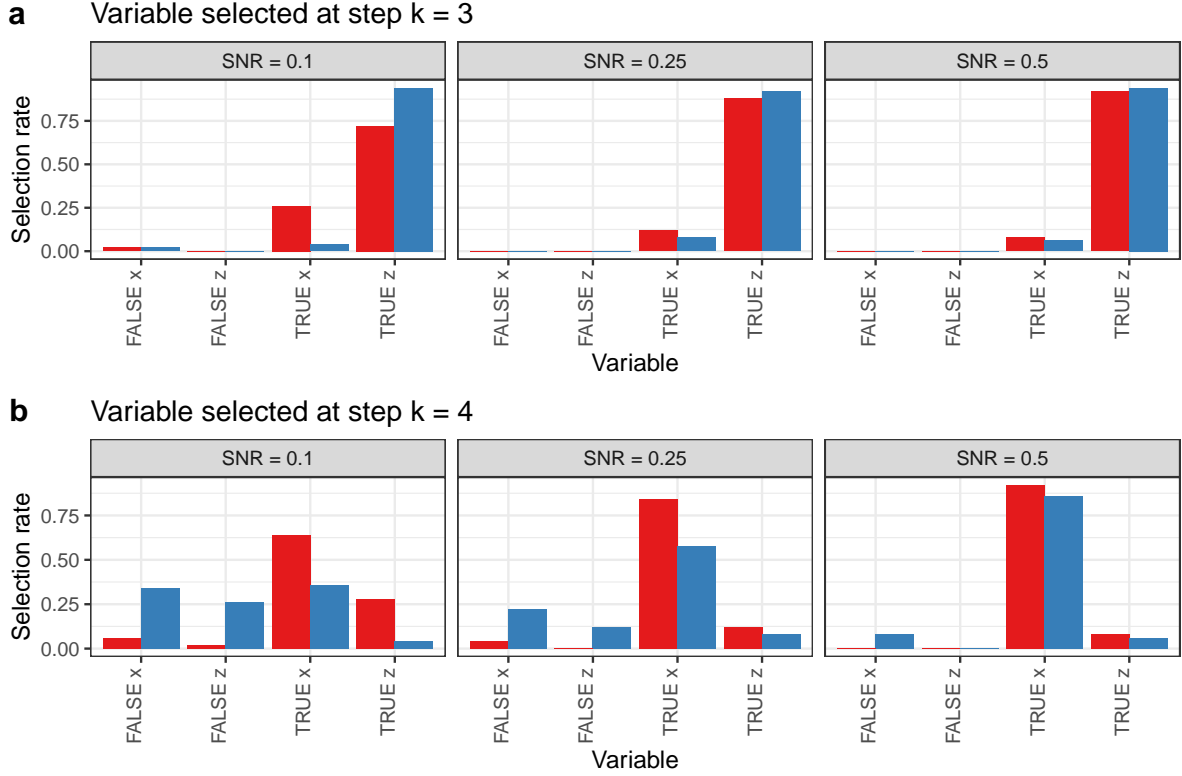


Figure S5: Variable selection accuracy in the supplementary model reduction experiment with different signal-to-noise ratios (SNR). **a-b)** Selection rate (proportion of times a given variable is selected) of each variable or variable type at step  $k$ , after the steps  $k = 1, 2$  that always correspond to the special baseline variables  $id$  and  $age$ , respectively. The red bars show the results for the greedy forward search, and blue bars for the predefined search path using ranking based on component relevances obtained via an additive variance decomposition. We see that in this experiment, for both methods, the true categorical variable  $z$  is the most common first free selection ( $k = 3$ ) and the true continuous variable is the most common second free selection ( $k = 4$ ). False selections are very rare at  $k = 3$ . At  $k = 4$ , the selection of a nuisance continuous variable (FALSE  $x$ ) is the most common wrong selection, and more prevalent when using the predefined search path (blue bars).

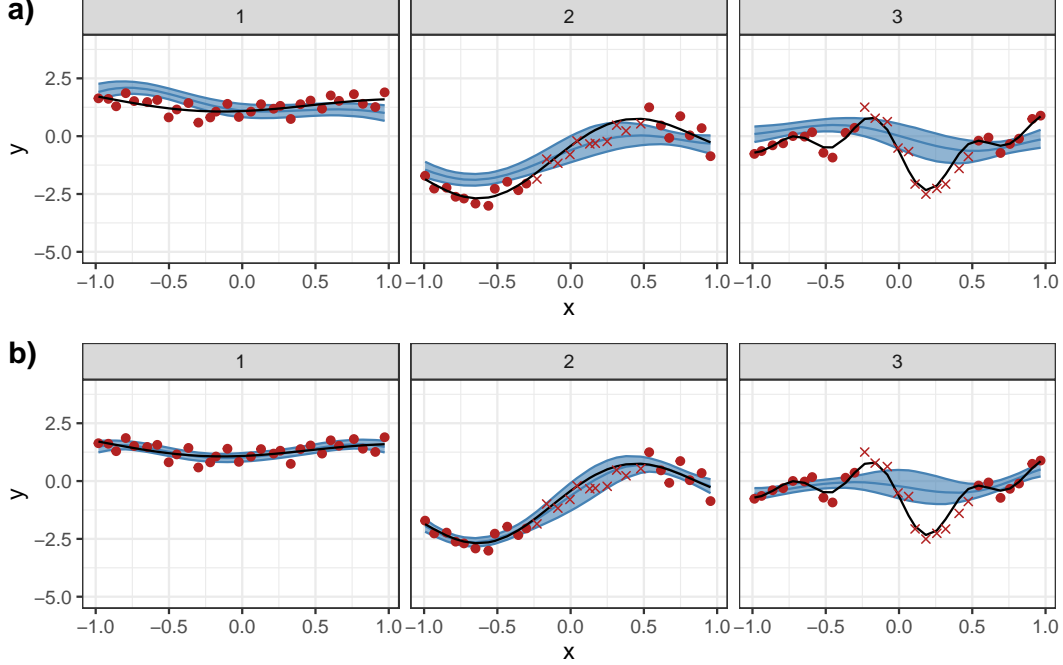


Figure S6: Kernel mismatch experiment. The blue ribbons and lines represent the posterior predictive distributions with median and 80% credible interval, using the kernels  $k_A$  and  $k_B$  in panels **a)** and **b)**, respectively. The three panels in each case correspond to values of  $z = 1, 2, 3$ . The red dots are training data, red crosses are test points. The black line is the oracle GP mean (Eq. 6) using the true kernel and  $\sigma_{\text{TRUE}}^2$  used to generate the data. Note that also the oracle kernel model is fit using only the training data.

which creates models with  $B = 30$  basis functions per group in each model term.

The simulated data and different model fits can be seen in Figure S6. We see that neither of the kernels A or B can capture the true covariance structure. Kernel  $k_A$  is the most limited one because it is forced to sum to zero over the categories. We do not recommend using it alone in practice, but together with the shared effect as in  $k_B$ , unless there is a known reason to use only  $k_A$ . An additional limitation of both  $k_A$  and  $k_B$  is that they cannot model the effects of the different categories with different lengthscales.

### S2.3 Practical scalability limit

We studied the practical scalability limit of the approximation strategy and the `lgpr2` implementation<sup>2</sup>. We simulated data in similar fashion as in Section S2.2, but with  $G = 10$  different groups. The fitted model is the same as `modelB` in Section S2.2. This means that the total number of basis functions is  $(G - 1)B + B = GB = 300$ . We generate  $10^2, 10^3, 10^4, 10^5$  observations for each group, which means a total number of  $N = 10^3, 10^4, 10^5, 10^6$  observations. The goal was to test whether model fitting is feasible and thus only one MCMC chain was run in each case with the number of both pre- and post warmup iterations being `iter` = 4, 40, 400.

Figure S7a shows that the runtime<sup>3</sup> grows linearly with data size, matching the theory. We see

<sup>2</sup>Package version 0.0.3.

<sup>3</sup>This experiment was run on a machine with a 4.20GHz Intel i7-7700K CPU with 16 GB RAM.

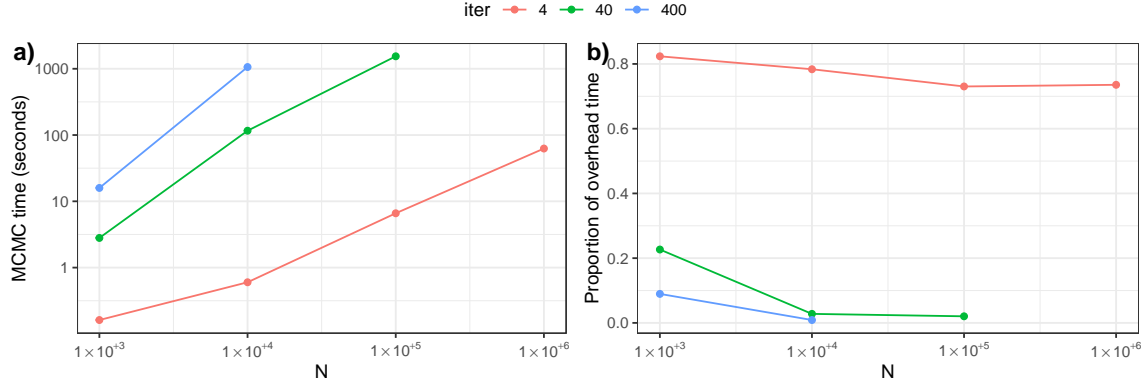


Figure S7: Practical scalability limit experiment. Panel a) shows the total MCMC runtime reported by Stan when running one chain with `iter` pre- and post-warmup iterations with different data sizes  $N$ . Panel b) shows what proportion of the entire wall clock time of model fitting using `lgpr2` that is attributed to factors other than running the MCMC algorithm. The amount of this overhead seems to shrink with the number of iterations and data size.

for example that with  $N = 10^4$ , the chain with `iter` = 400 can be run in  $\sim 0.3$  hours. Extrapolating linearly, the runtime would be  $\sim 3$  hours with  $N = 10^5$  and  $\sim 30$  hours with  $N = 10^6$ . However, it is unclear whether the linear relationship will hold in practice with very large data sizes, as practical limitations may appear. For MCMC to converge in Stan, we typically need chains that have `iter` on the order of 1000. In practice, memory will ultimately become an issue, since for example storing 1000 posterior predictive distribution draws at  $N = 10^6$  points will already take 8 GB of memory, as double precision floating point numbers are used.

In Figure S7b, we try to assess potential scalability-limiting factors that are independent of the MCMC algorithm. Such overhead factors could be for example reading and writing the data and the MCMC output. The proportion of this overhead time decreases as expected when longer chains are run. Additionally, we find that the proportion of overhead time slightly decreases with increasing data size, which leads us to believe that the overhead factors are not a bottleneck.

We estimate that fitting models to  $N = 10^5$  data points is viable using our implementation, which uses `CmdStanR` (Gabry et al., 2024) under the hood for MCMC inference. However, it greatly depends also on the total number of basis functions, as it affects the number of model parameters. Factors that affect the MCMC runtime of Stan are the posterior geometry and the cost of one gradient evaluation, as the gradient of the log posterior density is computed using automatic differentiation. Different inference algorithms and more efficient implementations specific to this model could potentially scale the method to millions of data points.

## S3 Supplementary methods

### S3.1 Approximate posterior predictive distribution

Recall from Section 4.1 of the main text that our approximation  $\tilde{\mathbf{f}} \approx \mathbf{f}$  is a linear model  $\tilde{\mathbf{f}} = \mathbf{\Psi}\boldsymbol{\xi}$  of the auxiliary parameters  $\boldsymbol{\xi}$ . Therefore instead of MCMC sampling directly from  $p(\tilde{\mathbf{f}}, \boldsymbol{\theta} \mid \mathcal{D})$ , we sample from  $p(\boldsymbol{\xi}, \boldsymbol{\theta} \mid \mathcal{D})$ . For a posterior draw  $(\boldsymbol{\xi}, \boldsymbol{\theta})$ , we can compute  $\mathbf{\Psi}$  using  $\boldsymbol{\theta}$  and create a draw from  $p(\tilde{\mathbf{f}} \mid \mathcal{D})$ . For out-of-sample test points  $\mathbf{x}_p^*$ ,  $p = 1, \dots, P$ , we can create a draw from the approximate posterior distribution of

$$\mathbf{f}^* = [f(\mathbf{x}_1^*), \dots, f(\mathbf{x}_P^*)]^\top \quad (2)$$

similarly as  $\tilde{\mathbf{f}}^* = \mathbf{\Psi}^* \boldsymbol{\xi}$ , where  $\mathbf{\Psi}^*$  is a  $P \times M$  matrix with elements  $[\mathbf{\Psi}^*]_{p,m} = \psi_m(\mathbf{x}_p^*)$ . Further, drawing from the observation distribution  $p(y \mid f(\mathbf{x}_p^*), \boldsymbol{\theta})$  then gives a draw from the posterior predictive distribution of observations at  $\mathbf{x}_p^*$ . Visualizations of the posterior predictive distribution in Figure 1 of main text, Figure S1 and Figure S2 have been done using this strategy.

#### S3.1.1 Componentwise approximate posteriors of additive GPs

For an additive GP, we can get a draw from the approximate marginal posterior of  $\mathbf{f}^{(j)}$  (Eq. 8) as  $\tilde{\mathbf{f}}^{(j)} = \mathbf{\Psi}^{(j)} \boldsymbol{\xi}$  where  $\mathbf{\Psi}^{(j)}$  denotes the matrix that is created by taking from  $\mathbf{\Psi}$  only the columns that correspond to component  $f^{(j)}$ . Analogously to Section S3.1, this can be done at test points. We have used this strategy to produce smooth visualizations of the marginal posteriors of different components in our result figures.

#### S3.1.2 Mean log predictive density

To measure model fit in Experiment 1, we computed the mean log predictive density at  $P$  test points  $\{(\mathbf{x}_p^*, y_p^*)\}_{p=1, \dots, P}$  as

$$\text{MPLD} = \frac{1}{SP} \sum_{s=1}^S \sum_{p=1}^P \log p(y_p^* \mid \boldsymbol{\theta}^{(s)}, f(\mathbf{x}_p^*)^{(s)})$$

where  $\boldsymbol{\theta}^{(s)}, \mathbf{f}^{*(s)} = [f(\mathbf{x}_1^*)^{(s)}, \dots, f(\mathbf{x}_P^*)^{(s)}]$ ,  $s = 1, \dots, S$ , are draws from  $p(\boldsymbol{\theta}, \mathbf{f}^* \mid \mathcal{D})$  and

$$p(y \mid \boldsymbol{\theta}, f(\mathbf{x})) = \mathcal{N}(y \mid f(\mathbf{x}), \sigma^2) \quad (3)$$

since we used the Gaussian likelihood model. For the exact model, the draws were generated so that for each posterior draw from  $p(\boldsymbol{\theta} \mid \mathcal{D})$  given by MCMC,  $\mathbf{f}^*$  was drawn from  $p(\mathbf{f}^* \mid \boldsymbol{\theta}, \mathcal{D})$ , which has an analytical expression (see Section S3.2) below. For the approximate models, the draws were from the corresponding approximate posterior, obtained using the strategy described above in Section S3.1.

### S3.2 Exact GP regression under Gaussian observation model

#### S3.2.1 Model inference

We focus here on the Gaussian observation model where  $p(y_n \mid f(\mathbf{x}_n), \sigma^2) = \mathcal{N}(y_n \mid f(\mathbf{x}_n), \sigma^2)$  independently for all  $n = 1, \dots, N$ , and the noise variance  $\sigma^2$  is part of the parameter vector  $\boldsymbol{\theta}$ . The marginal likelihood  $p(\mathbf{y} \mid \boldsymbol{\theta})$  has the analytical form

$$p(\mathbf{y} \mid \boldsymbol{\theta}) = \int p(\mathbf{y} \mid \mathbf{f}, \boldsymbol{\theta}) p(\mathbf{f} \mid \boldsymbol{\theta}) d\mathbf{f} = \mathcal{N}(\mathbf{0}, \mathbf{K} + \sigma^2 \mathbf{I}) \quad (4)$$

where  $\mathbf{f}$  has been analytically marginalized out (Rasmussen and Williams, 2006) and  $\mathbf{K}$  denotes the  $N \times N$  kernel matrix between training points, with elements  $\{\mathbf{K}\}_{i,j} = k(\mathbf{x}_i, \mathbf{x}_j)$ . We can sample just the marginal posterior  $p(\boldsymbol{\theta} \mid \mathcal{D}) \propto p(\mathbf{y} \mid \boldsymbol{\theta})p(\boldsymbol{\theta})$  with MCMC, as it is more efficient than sampling the joint posterior  $p(\boldsymbol{\theta}, \mathbf{f} \mid \mathcal{D})$ , even though it still has the  $\mathcal{O}(N^3)$  scaling that comes from evaluating the  $N$ -dimensional normal density  $\mathcal{N}(\mathbf{0}, \mathbf{K} + \sigma^2 \mathbf{I})$ . Joint posterior samples  $(\boldsymbol{\theta}^{(s)}, \mathbf{f}^{(s)})$  can be obtained so that for each MCMC draw  $\boldsymbol{\theta}^{(s)}$ , vector  $\mathbf{f}^{(s)}$  is drawn from  $p(\mathbf{f} \mid \boldsymbol{\theta}, \mathcal{D}) = \mathcal{N}(\boldsymbol{\mu}, \boldsymbol{\Sigma})$ , where

$$\begin{cases} \boldsymbol{\mu} &= \mathbf{K} \mathbf{K}_y^{-1} \mathbf{y} \\ \boldsymbol{\Sigma} &= \mathbf{K} - \mathbf{K} \mathbf{K}_y^{-1} \mathbf{K}^\top, \end{cases} \quad (5)$$

and  $\mathbf{K}_y = \mathbf{K} + \sigma^2 \mathbf{I}$ .

### S3.2.2 Prediction

For  $\mathbf{f}^*$ , defined as in Eq. 2, we have  $p(\mathbf{f}^* \mid \boldsymbol{\theta}, \mathcal{D}) = \mathcal{N}(\boldsymbol{\mu}_*, \boldsymbol{\Sigma}_*)$  with

$$\begin{cases} \boldsymbol{\mu}_* &= \mathbf{K}_* \mathbf{K}_y^{-1} \mathbf{y} \\ \boldsymbol{\Sigma}_* &= \mathbf{K}_{**} - \mathbf{K}_* \mathbf{K}_y^{-1} \mathbf{K}_*^\top, \end{cases} \quad (6)$$

where  $\mathbf{K}_*$  is the  $P \times N$  kernel matrix between test points and training points, and  $\mathbf{K}_{**}$  is the  $P \times P$  kernel matrix between test points. The predictive distribution (conditional on parameters  $\boldsymbol{\theta}$ ) for observations at the  $P$  test points is

$$p(\mathbf{y}^* \mid \boldsymbol{\theta}, \mathcal{D}) = \mathcal{N}(\boldsymbol{\mu}^*, \boldsymbol{\Sigma}^* + \sigma^2 \mathbf{I}), \quad (7)$$

where  $\mathbf{f}^*$  has been analytically marginalized out. See for example Rasmussen and Williams (2006) for derivations. In an additive GP model, also the posterior of any component  $j$  is multivariate Gaussian  $p(\mathbf{f}^{*(j)} \mid \boldsymbol{\theta}, \mathcal{D}) = \mathcal{N}(\boldsymbol{\mu}_*^{(j)}, \boldsymbol{\Sigma}_*^{(j)})$

$$\begin{cases} \boldsymbol{\mu}_*^{(j)} &= \mathbf{K}_*^{(j)} \mathbf{K}_y^{-1} \mathbf{y} \\ \boldsymbol{\Sigma}_*^{(j)} &= \mathbf{K}_{**}^{(j)} - \mathbf{K}_*^{(j)} \mathbf{K}_y^{-1} \mathbf{K}_*^{(j)\top}, \end{cases} \quad (8)$$

where  $\mathbf{K}_*^{(j)}$  is the kernel matrix of the  $j$ th component between test points and training points, and  $\mathbf{K}_{**}^{(j)}$  is the kernel matrix of the  $j$ th component between the test points. See for example Timonen et al. (2021) for derivations. As these analytical expressions are available, we can use the same strategy as described in Section S3.2.1 above to draw from the joint posterior of  $\boldsymbol{\theta}$  and  $\mathbf{f}^*$ ,  $\mathbf{y}^*$  or any  $\mathbf{f}^{*(j)*}$ .

### S3.3 Approximate GP regression with $\mathbf{f}$ marginalized out

In some applications, inference under the Gaussian observation model can be easier using the marginalization approach also for the approximate model. This is due to the reduced parameter dimension, even though the theoretical complexity will be worse. With our approximation  $\mathbf{K} \approx \tilde{\mathbf{K}} = \boldsymbol{\Psi} \boldsymbol{\Psi}^\top$ , where  $\boldsymbol{\Psi}$  has size  $N \times M$  with  $M < N$ , we have

$$\log p(\mathbf{y} \mid \boldsymbol{\theta}) \approx \log \mathcal{N}(\mathbf{y} \mid \mathbf{0}, \tilde{\mathbf{K}}_y) = -\frac{N}{2} \log(2\pi) - \frac{1}{2} \log |\tilde{\mathbf{K}}_y| - \frac{1}{2} \mathbf{y}^\top \tilde{\mathbf{K}}_y^{-1} \mathbf{y}, \quad (9)$$

where  $\tilde{\mathbf{K}}_y = \tilde{\mathbf{K}} + \sigma^2 \mathbf{I}$ . We can efficiently compute the log determinant and the quadratic form of the inverse of  $\tilde{\mathbf{K}}_y$  with the help of Eq. 16 and Eq. 17, as

$$\mathbf{y}^\top \tilde{\mathbf{K}}_y^{-1} \mathbf{y} = \frac{1}{\sigma^2} \left( \mathbf{y}^\top \mathbf{y} - \mathbf{z}^\top \mathbf{Z}^{-1} \mathbf{z} \right) \quad (10)$$

$$\log |\tilde{\mathbf{K}}_y| = 2 \cdot (N - M) \cdot \log \sigma + \log |\mathbf{Z}| \quad (11)$$



where  $\mathbf{Z} = \sigma^2 + \mathbf{\Psi}^\top \mathbf{\Psi}$  and  $\mathbf{z} = \mathbf{\Psi}^\top \mathbf{y}$ . The computational cost then comes from evaluating  $\log |\mathbf{Z}|$  and  $\mathbf{z}^\top \mathbf{Z}^{-1} \mathbf{z}$  and the complexity is  $\mathcal{O}(NM^2)$ . Because this is a worse theoretical scaling than that of the approach involving auxiliary variables  $\boldsymbol{\xi}$ , we have not used this approach in our experiments.

### S3.4 Derivation of Equation 35 of main text

$$\begin{aligned}
[\mathbf{S}]_{l,m} &= \int_{\Omega} \phi_l''(x) \phi_m''(x) dx \\
&= \frac{\pi^4 l^2 m^2}{(2L)^4} \int_{\Omega} \phi_l(x) \phi_m(x) dx \\
&= \frac{\pi^4 l^2 m^2}{16L^5} \int_{-L}^L \sin\left(\frac{\pi l(x+L)}{2L}\right) \sin\left(\frac{\pi m(x+L)}{2L}\right) dx \\
&= \frac{\pi^4 l^2 m^2}{16L^5} \cdot \frac{2L}{\pi} \cdot \frac{m \cos(m\pi) \sin(l\pi) - l \cos(l\pi) \sin(m\pi)}{l^2 - m^2} \\
&= 0
\end{aligned}$$

for  $l \neq m$ .

### S3.5 Practical considerations

Notice that all functions  $\psi_m(\mathbf{x})$  that we presented in Section 2 of the main text were of the form  $\psi_m(\mathbf{x}) = \sqrt{\delta_m} \cdot \psi_m^\dagger(\mathbf{x})$ , where  $\delta_m$  depends on the parameters  $\boldsymbol{\theta}$  but  $\psi_m^\dagger(\mathbf{x})$  does not. Therefore  $\mathbf{\Psi} = \mathbf{\Psi}^\dagger \mathbf{\Delta}$  where  $\mathbf{\Delta}$  is the  $M \times M$  diagonal matrix containing the values  $\sqrt{\delta_m}$ ,  $m = 1, \dots, M$  on the diagonal. The  $N \times M$  matrix  $\mathbf{\Psi}^\dagger$ , which has elements  $\{\mathbf{\Psi}^\dagger\}_{n,m} = \psi_m^\dagger(\mathbf{x}_n)$ , is independent of parameters and needs to be computed only once during parameter inference.

### S3.6 Multivariate normal distribution

The  $N$ -dimensional zero-mean multivariate normal density is

$$\mathcal{N}(\mathbf{y} \mid \mathbf{0}, \mathbf{\Sigma}) = (2\pi)^{-\frac{N}{2}} |\mathbf{\Sigma}|^{-\frac{1}{2}} \exp\left(-\frac{1}{2} \mathbf{y}^\top \mathbf{\Sigma}^{-1} \mathbf{y}\right) \quad (12)$$

and its log density is

$$\log \mathcal{N}(\mathbf{y} \mid \mathbf{0}, \mathbf{\Sigma}) = -\frac{N}{2} \log(2\pi) - \frac{1}{2} \log |\mathbf{\Sigma}| - \frac{1}{2} \mathbf{y}^\top \mathbf{\Sigma}^{-1} \mathbf{y}, \quad (13)$$

where both of the last two terms have an  $\mathcal{O}(N^3)$  computation complexity.

### S3.7 Matrix identities

Consider an  $N \times M$  matrix  $\mathbf{V}$ , an invertible  $M \times M$  matrix  $\mathbf{D}$ , and a symmetric invertible  $N \times N$  matrix  $\mathbf{S}$ . Then using the Woodbury matrix identity and the determinant lemma (see for example [Press et al. \(2007\)](#)), we get

$$(\mathbf{S} + \mathbf{V} \mathbf{D} \mathbf{V}^\top)^{-1} = \mathbf{S}^{-1} - \mathbf{S}^{-1} \mathbf{V} (\mathbf{D}^{-1} + \mathbf{V}^\top \mathbf{S}^{-1} \mathbf{V})^{-1} (\mathbf{S}^{-1} \mathbf{V})^\top \quad (14)$$

$$|\mathbf{S} + \mathbf{V} \mathbf{D} \mathbf{V}^\top| = |\mathbf{D}^{-1} + \mathbf{V}^\top \mathbf{S}^{-1} \mathbf{V}| \cdot |\mathbf{D}| \cdot |\mathbf{S}|. \quad (15)$$

By setting  $\mathbf{S} = \sigma^2 \mathbf{I}$ , we get

$$\left(\sigma^2 \mathbf{I} + \mathbf{V} \mathbf{D} \mathbf{V}^\top\right)^{-1} = \frac{1}{\sigma^2} \left(\mathbf{I} - \mathbf{V} \mathbf{Z}^{-1} \mathbf{V}^\top\right) \quad (16)$$

$$\left|\sigma^2 \mathbf{I} + \mathbf{V} \mathbf{D} \mathbf{V}^\top\right| = \sigma^{2(N-M)} \cdot |\mathbf{Z}| \cdot |\mathbf{D}|, \quad (17)$$

where  $\mathbf{Z} = \sigma^2 \mathbf{D}^{-1} + \mathbf{V}^\top \mathbf{V}$ .

## References

- B. Carpenter, A. Gelman, M. D. Hoffman, D. Lee, B. Goodrich, M. Betancourt, M. Brubaker, J. Guo, P. Li, and A. Riddell. Stan: A probabilistic programming language. *Journal of Statistical Software*, 76(1):1–32, 2017.
- J. Gabry, R. Češnovar, A. Johnson, and S. Bröder. *cmdstanr: R Interface to 'CmdStan'*, 2024. URL <https://mc-stan.org/cmdstanr/>. R package version 0.8.1.9000, <https://discourse.mc-stan.org>.
- W. H. Press, S. A. Teukolsky, W. T. Vetterling, and B. P. Flannery. *Numerical Recipes 3rd Edition: The Art of Scientific Computing*. Cambridge University Press, USA, 3rd edition, 2007.
- C. E. Rasmussen and C. K. I. Williams. *Gaussian Processes for Machine Learning*. MIT Press, Cambridge, Massachusetts, 2006.
- Stan Development Team. *Stan Reference Manual, Version 2.35*, 2024. URL <https://mc-stan.org/docs/reference-manual/mcmc.html>. Accessed: 2024-09-06.
- J. Timonen, H. Mannerström, A. Vehtari, and H. Lähdesmäki. lgpr: an interpretable non-parametric method for inferring covariate effects from longitudinal data. *Bioinformatics*, 37(13):1860–1867, 2021.